Exp Astron
DOI 10.1007/s10686-013-9344-3

ORIGINAL ARTICLE

XIPE: the X-ray imaging polarimetry explorer

Paolo Soffitta · Xavier Barcons · Ronaldo Bellazzini · João Braga · Enrico Costa · George W. Fraser · Szymon Gburek · Juhani Huovelin · Giorgio Matt · Mark Pearce · Juri Poutanen · Victor Reglero · Andrea Santangelo · Rashid A. Sunyaev · Gianpiero Tagliaferri · Martin Weisskopf · Roberto Aloisio · Elena Amato · Primo Attiná · Magnus Axelsson · Luca Baldini · Stefano Basso · Stefano Bianchi · Pasquale Blasi · Johan Bregeon · Alessandro Brez · Niccoló Bucciantini · Luciano Burderi · Vadim Burwitz · Piergiorgio Casella · Eugene Churazov · Marta Civitani · Stefano Covino · Rui Miguel Curado da Silva · Giancarlo Cusumano · Mauro Dadina · Flavio D'Amico · Alessandra De Rosa · Sergio Di Cosimo · Giuseppe Di Persio · Tiziana Di Salvo · Michal Dovciak · Ronald Elsner · Chris J. Eyles · Andrew C. Fabian · Sergio Fabiani · Hua Feng · Salvatore Giarrusso · René W. Goosmann · Paola Grandi · Nicolas Grosso · Gianluca Israel · Miranda Jackson · Philip Kaaret · Vladimir Karas · Michael Kuss · Dong Lai · Giovanni La Rosa · Josefin Larsson · Stefan Larsson · Luca Latronico · Antonio Maggio · Jorge Maia · Frédéric Marin · Marco Maria Massai · Teresa Mineo · Massimo Minuti · Elena Moretti · Fabio Muleri · Stephen L. O'Dell · Giovanni Pareschi · Giovanni Peres · Melissa Pesce · Pierre-Olivier Petrucci · Michele Pinchera · Delphine Porquet · Brian Ramsey · Nanda Rea · Fabio Reale · Juana Maria Rodrigo · Agata Różańska · Alda Rubini · Pawel Rudawy · Felix Ryde · Marco Salvati · Valdivino Alexandre de Santiago Jr. · Sergey Sazonov · Carmelo Sgró · Eric Silver · Gloria Spandre · Daniele Spiga · Luigi Stella · Toru Tamagawa · Francesco Tamborra · Fabrizio Tavecchio · Teresa Teixeira Dias · Matthew van Adelsberg · Kinwah Wu · Silvia Zane

Received: 21 April 2013 / Accepted: 16 July 2013

E. Costa · A. De Rosa · S. Di Cosimo · G. Di Persio · S. Fabiani · F. Muleri · A. Rubini · P. Soffitta (✉)
IAPS/INAF, Via Fosso del Cavaliere 100, 00133 Rome, Italy
e-mail: paolo.soffitta@iaps.inaf.it

X. Barcons
Instituto de Física de Cantabria (CSIC-UC), Avenida de los Castros, s/n,
39005 Santander Cantabria, Spain

R. Bellazzini · J. Bregeon · A. Brez · L. Latronico · M. Kuss · M. Minuti · M. Pesce · M. Pinchera · C. Sgró · G. Spandre
INFN-Pisa, Largo B. Pontecorvo 3, 56127 Pisa, Italy

J. Braga · F. D'Amico · V. A. de Santiago Jr.
INPE Div de Astrofsica, Av dos Astronautas 1758 Jd. Granja - CEP: 12227-010,
São José dos Campos, SP, Brazil

Published online: 24 August 2013

G. W. Fraser
Department of Physics and Astronomy, University of Leicester, Space Research Centre, Leicester, LE1 7RH, UK

S. Gburek
Solar Physics Division, Space Research Centre, Polish Academy of Sciences, 51-622 Wroclaw, ul. Kopernika, Poland

J. Huovelin
Department of Physics, University of Helsinki, Erik Palmenin aukio 1, 00014 Finland

S. Bianchi · G. Matt · F. Tamborra
Dipartimento di Física "E. Amaldi", Universita' degli Studi Roma Tre, Via della Vasca Navale 84, 00146 Rome, Italy

M. Axelsson · M. S. Jackson · J. Larsson · S. Larsson · E. Moretti · M. Pearce · F. Ryde
Department of Physics, KTH, Royal Institute of Technology, Stockholm, Sweden

M. Axelsson · M. S. Jackson · J. Larsson · S. Larsson · E. Moretti · M. Pearce · F. Ryde
The Oskar Klein Centre for Cosmoparticle Physics, AlbaNova University Centre, Stockholm, Sweden

J. Poutanen
Department of Physics, Astronomy Division, University of Oulu, PO Box 3000, 90014, Oulu, Finland

V. Reglero · J. M. Rodrigo
Instituto de Ciencias de los Materiales, Universidad de Valencia, Astronomia i Astrofísica, Dr Moliner 50, 46100 Burjassot, Spain

A. Santangelo
Iniversität Tübingen, Institut für Astronomie und Astrophysik, Sand 1, 72076 Tübingen, Germany

E. Churazov · R. A. Sunyaev
Max-Planck-Institut für Astrophysik, Karl-Schwarzschild-Str. 1, 85748 Garching, Germany

S. Basso · M. Civitani · S. Covino · D. Spiga · G. Pareschi · G. Tagliaferri · F. Tavecchio
INAF/Osservatorio Astronomico di Brera, Via E. Bianchi 46, 23807 Merate, Lc, Italy

R. Elsner · S. L. O'Dell · B. Ramsey · M. Weisskopf
NASA Marshall Space Flight Center, 320 Sparkman Drive NW, Huntsville, AL 35805-1912, USA

P. Attiná
Thales Alenia Space-Italia s.p.a., Strada Antica di Collegno 253, 10146 Turin, Italy

L. Baldini · M. M. Massai
Dipartimento di Física, Universita' di Pisa & INFN-Pisa, Largo Pontecorvo, 3 56127, Pisa, Italy

R. Aloisio · E. Amato · P. Blasi · N. Bucciantini · M. Salvati
INAF/Osservatorio Astrofisico di Arcetri, Largo Enrico Fermi, 50125 Florence, Italy

L. Burderi
Dipartimento di Fisica, Università di Cagliari, SP Monserrato-Sestu km 0.7, 09042 Cagliari, Italy

V. Burwitz
Max-Planck-Institut für extraterrestrische Physik, 85741 Garching, Germany

V. Burwitz
Panter X-ray test facility, Gautinger Str. 45, 82061 Neuried, Germany

P. Casella · G. Israel · L. Stella
INAF/Osservatorio Astrofisico di Roma, Via di Frascati, 33, 00040 Rome, Italy

R. M. Curado da Silva · J. Maia · T. Teixeira Dias
Departimento de Física, Coimbra Universidad Portugal, 3004-516, Coimbra, Portugal

G. Cusumano · S. Giarrusso · G. La Rosa · T. Mineo
INAF/IASF-Palermo, Via Ugo La Malfa 153, 90146 Palermo, Italy

M. Dadina · P. Grandi
INAF/IASF-Bologna, via Gobetti 101, 40129 Bologna, Italy

T. Di Salvo · G. Peres · F. Reale
DiFC, Universita degli Studi di Palermo, via Archirafi 36, 90123 Palermo, Italy

M. Dovciak · V. Karas
Astronomical Institute, Academy of Sciences of the Czech Republic, Bocni II 1401, 14131 Prague, Czech Republic

C. J. Eyles
School of Physics and Astronomy, University of Birmingham, B152TT Birmingham, UK

H. Feng
Department of Engineering Physics & Center for Astrophysics, Tsinghua University, 100084 Beijing, China

A. C. Fabian
Institute of Astronomy, University of Cambridge, Madingley Rd, CB3 0HA Cambridge, UK

R. W. Goosmann · N. Grosso · F. Marin · D. Porquet
Observatoire Astronomique de Strasbourg, 11 rue de l'université, 67000 Strasbourg, France

P. Kaaret
Department of Physics and Astronomy, University of Iowa, Iowa City, IA 52242 USA

D. Lai
Cornell University, Space Sciences Bldg., Ithaca, NY 14853, USA

A. Maggio
INAF/Osservatorio Astronomico di Palermo, Piazza del Parlamento 1, 90134 Palermo, Italy

P.-O. Petrucci
Institut de Planétologie et d'Astrophysique de Grenoble (IPAG), UJF-Grenoble 1 /CNRS-INSU UMR 5274, Grenoble 38041, France

N. Rea
Institute of Space Sciences, CSIC-IEEC; Facultat de Ciencies, 08193 Barcelona, Spain

A. Różańska
Polish Academy of Sciences, Nicolaus Copernicus Astronomical Centre, Bartycka 18, 00-716 Warsaw, Poland

P. Rudawy
Astronomical Institute, Wroclaw University, Kopernika 11, 51-622 Wroclaw, Poland

Abstract X-ray polarimetry, sometimes alone, and sometimes coupled to spectral and temporal variability measurements and to imaging, allows a wealth of physical phenomena in astrophysics to be studied. X-ray polarimetry investigates the acceleration process, for example, including those typical of magnetic reconnection in solar flares, but also emission in the strong magnetic fields of neutron stars and white dwarfs. It detects scattering in asymmetric structures such as accretion disks and columns, and in the so-called molecular torus and ionization cones. In addition, it allows fundamental physics in regimes of gravity and of magnetic field intensity not accessible to experiments on the Earth to be probed. Finally, models that describe fundamental interactions (e.g. quantum gravity and the extension of the Standard Model) can be tested. We describe in this paper the X-ray Imaging Polarimetry Explorer (XIPE), proposed in June 2012 to the first ESA call for a small mission with a launch in 2017. The proposal was, unfortunately, not selected. To be compliant with this schedule, we designed the payload mostly with existing items. The XIPE proposal takes advantage of the completed phase A of POLARIX for an ASI small mission program that was cancelled, but is different in many aspects: the detectors, the presence of a solar flare polarimeter and photometer and the use of a light platform derived by a mass production for a cluster of satellites. XIPE is composed of two out of the three existing JET-X telescopes with two Gas Pixel Detectors (GPD) filled with a He-DME mixture at their focus. Two additional GPDs filled with a 3-bar Ar-DME mixture always face the Sun to detect polarization from solar flares. The Minimum Detectable Polarization of a 1 mCrab source reaches 14 % in the 2–10 keV band in 10^5 s for pointed observations, and 0.6 % for an X10 class solar flare in the 15–35 keV energy band. The imaging capability is 24 arcsec Half Energy Width (HEW) in a Field of View of 14.7 arcmin $\times$ 14.7 arcmin. The spectral resolution is 20 % at 6 keV and the time resolution is 8 μs. The imaging capabilities of the JET-X optics and of the GPD have been demonstrated by a recent calibration campaign at PANTER X-ray test facility of the Max-Planck-Institut für extraterrestrische Physik

S. Sazonov
Space Research Institute, Russian Academy of Sciences, Profsoyuznaya 84/32, 117997 Moscow, Russia

S. Sazonov
Moscow Institute of Physics and Technology, Institutsky per. 9, 141700 Dolgoprudny, Russia

E. Silver
Harvard-Smithsonian Center For Astrophysics, 60 Garden Street, Cambridge, MA 02138 USA

T. Tamagawa
RIKEN, 2-1 Hirosawa, Wako, Saitama 351-0198, Japan

M. van Adelsberg
Centre for Relativistic Astrophysics, Georgia Institute of Technology, 837 State Street, Atlanta, GA 30332, USA

K. Wu · S. Zane
Mullard Space Science Laboratory, University College London, Holmbury St Mary, RH5 6NT Dorking, UK

(MPE, Germany). XIPE takes advantage of a low-earth equatorial orbit with Malindi as down-link station and of a Mission Operation Center (MOC) at INPE (Brazil). The data policy is organized with a Core Program that comprises three months of Science Verification Phase and 25 % of net observing time in the following 2 years. A competitive Guest Observer program covers the remaining 75 % of the net observing time.

Keywords Astronomy · X-ray · Polarimetry

1 Introduction

In 50 years of X-ray astronomy, instrumentation has achieved fantastic advancements in imaging (*Chandra*), timing (*Rossi X-ray Timing Explorer*, *RXTE*) and spectroscopy (*Chandra* and *XMM-Newton*). No equivalent progress has been achieved in X-ray polarimetry, despite the fact that the key to uncover a number of scientific questions in fundamental physics and the behavior of matter under extreme conditions is encoded uniquely in this largely unexplored degree of freedom of high-energy radiation. In spite of the lack of fresh data, solid theoretical developments suggest that a wealth of important issues on the physics of X-ray sources could be solved by measuring their linear polarization.

At the beginning of X-ray astronomy, polarimeters were flown aboard rockets [2, 87] and aboard the OSO-8 [86, 135] and ARIEL-5 [36] satellites. The only positive detection was the polarization of the Crab Nebula [138] and two significant upper limits were obtained on Cyg X-1 [136] and Sco X-1 [137], plus many other upper limits of modest significance [47]. The introduction of X-ray optics, while producing a dramatic improvement in sensitivity, removed the need to rotate the satellite. Therefore, polarimetry based on the classical techniques, Bragg diffraction and Thomson scattering (which require rotation), became seriously mismatched with imaging and spectroscopy. As a result, no polarimeters were included in major X-ray missions by NASA or ESA. Non-solar hard X-ray polarimeters based on Compton effect resulted in a number of balloon-borne narrow field experiments [39, 68, 92] and in a polarimeter for Gamma Ray Bursts [142] on-board the solar-power sail demonstrator *IKAROS*.

In the last 10 years, with the development of sensors based on the photoelectric effect [19], polarimetry has been again considered as a realistic option, either for large telescopes with swappable instrumentation or for dedicated small missions. An intense activity of theoretical modeling has started again. A polarimetry mission, POLARIX [20], was one of two selected for flight after a phase A study following an ASI AO issued in 2008 for a small mission. The program was subsequently cancelled. Soon after, in 2009, NASA approved the Gravity and Extreme Magnetism Small Explorer (GEMS, [45, 49, 121]), a small size satellite to perform X-ray polarimetry, to be launched in 2014. Just at the end of May 2012, NASA decided to discontinue GEMS for programmatic reasons. A polarimetry mission based on instrumentation

already existing or of high technical readiness level became, therefore, very timely. The X-ray Imaging Polarimetry Explorer (XIPE) fulfils these requirements. It is based on already existing items, namely two out of three X-ray Mirror Modules built, tested and calibrated for the JET-X project [17, 141] and never flown (a fourth one is now operating well on the Swift satellite [14]) and the GPDs studied for more than 10 years [8, 9, 80, 81, 114] and extensively tested for POLARIX and for XEUS/IXO (*X-ray Evolving Universe Spectroscopy then evolved in International X-ray Observatory*, [6]). The photon by photon approach of the GPDs and the wide Field of View (FoV, 14.7 arcmin $\times$ 14.7 arcmin) are compatible with a satellite of modest performance in terms of attitude control.

An extremely robust and relatively cheap bus used for communication satellites, the Iridium NEXT, can harbor XIPE without modification. XIPE can perform polarimetry of tens of X-ray sources combined with imaging (24 arcseconds HEW resolution), spectroscopy of continuum (20 % @ 6 keV) and timing (8 μs resolution). XIPE's unique results enable us to explore the physics in extreme magnetic fields (in isolated or accreting pulsars) and in extreme gravitational fields (in neutron stars and black holes), to study the acceleration of particles in shocks in supernova remnants and to study the disk and the onset of jets in μquasars. A sample of extragalactic objects can also be probed, especially Blazars. Due to the high readiness of the technology, we are also proposing to perform polarimetry of solar flares, which will provide a clue to understanding the physics of magnetic reconnection.

XIPE opens a new window in high energy astrophysics and offers a large discovery space. Tests of fundamental physics can be performed using the Universe as a laboratory with extreme phenomenology related to General Relativity, the measure of the spin of black holes, or to QED, the detection of effects of vacuum polarization in extreme magnetic fields. Last but not least, XIPE could search for the birefringence predicted by Loop Quantum Gravity Theories or by theories of axion-like particles: one of the less exotic but most elusive candidates for Dark Matter.

The breakthrough results promised by XIPE well fit the themes of ESA Cosmic Vision: 2.1 *From the Sun to the edge of the Solar System*; 3.1 *Explore the limits of contemporary physics*; 3.3 *Matter under extreme conditions* and 4.3 *The evolving violent Universe*, and are far beyond what could be expected from a small mission. This is only possible because we can use instrumentation of high performance and demonstrated maturity, including a calibration of one GPD at the focus of an X-ray JET-X optics at the PANTER X-ray test facility. Such instrumentation, in large part, already exists.

2 Astrophysics with XIPE

XIPE, while proposing to install the same X-ray optics of POLARIX [20], takes advantage of a new detector design [10, 82] involving a larger body with improved control of the electric field and of the space distribution of the residual background [113], and is also capable of measuring polarization of radiation emitted by solar flares by means of a GPD with an extended energy band up to 35 keV, and to make high time resolution photometry. Moreover, the proposed platform is directly derived

from those of a cluster of satellites for telecommunication. The platform is lighter and includes the option of transmission using the X-band.

The astrophysical goals of XIPE, except in the case of solar flares, follow the line of what is already proposed for POLARIX. Hereafter, we summarize only the main theoretical expectations, including new updates and the expected sensitivity in terms of Minimum Detectable Polarization (MDP, see (1)).

2.1 Acceleration phenomena

Acceleration phenomena in Supernova Remnants are believed to be responsible for the production of the bulk of the cosmic rays reaching the Earth, while jetted Active Galactic Nuclei (AGNs) [95, 96] are a possible source of Ultra High Energy Cosmic Rays. X-rays are emitted close to the region of the maximum possible acceleration by means of the synchrotron mechanism by electrons that then rapidly lose their energy. X-ray polarimetry probing the environment close to the acceleration site is therefore a powerful tool to investigate the acceleration phenomena.

– **Supernova remnants** Supernova Remnants (SNRs) are believed to be the acceleration sites of cosmic rays up to 10^{15} eV. While the line emission makes it possible to determine the state of ionization of its thermal plasma, the lack, or the weakness, of emission lines is generally believed to be due to acceleration mechanisms responsible for the synchrotron emission or non thermal bremsstrahlung. Moreover, TeV emission from some SNRs supports the idea that in some regions, electrons are energized at least up to TeV. Imaging polarimetry in this regard is useful to localize the regions of shock acceleration and to measure the strength and the orientation of the magnetic field at these emission sites [133]. Probing the regions where thermal or nonthermal plasma is emitting in X-rays is particularly important in *small size* SNRs like Cas A, Tycho and *Kepler* (see e.g. [3, 133] and see Fig. 1). *The high X-ray polarization expected where the synchrotron process is prevalent (e.g. in the filaments usually located on the shell boundaries) should be much reduced where the non-thermal emission is just a fraction of the thermal one. However in the SNR 1006 radio polarization* [103] *showed that where the synchrotron is prevalent (e.g. in the two bright radio and X-ray lobes NE and SW) the measured degree of radio polarization is just 17 % and this is probably due to a locally disordered magnetic field. Instead in regions where non-thermal emission is not prevailing as in the SE rim the measured polarization is 60 % possibly indicating a highly oriented magnetic field. Such considerations may be applied to Cas A for which there is an indication of the presence of a tangential magnetic field at its outer edges* [35]. *We note that in this source (*[11] *but see also* [28]*) in the spectral region between 4 and 6 keV the power-law component is about 22.5 % of the total emission while between 8 and 10 keV this component is 50 %. Being the equivalent width of the iron line about 1 keV the fraction of the power-law component between 6 and 8 keV is a non-negligible 19 %. With one long (1 Ms) look of Cas A, the MDP is 1.6 % (4–6 keV), 3.5 % (6–8 keV) and 11.7 % (8–10 keV) or 4.3 %, 10.5 % and 35 % in each of the 9 subregions that we can think to divide Cas A. Giving the estimated*

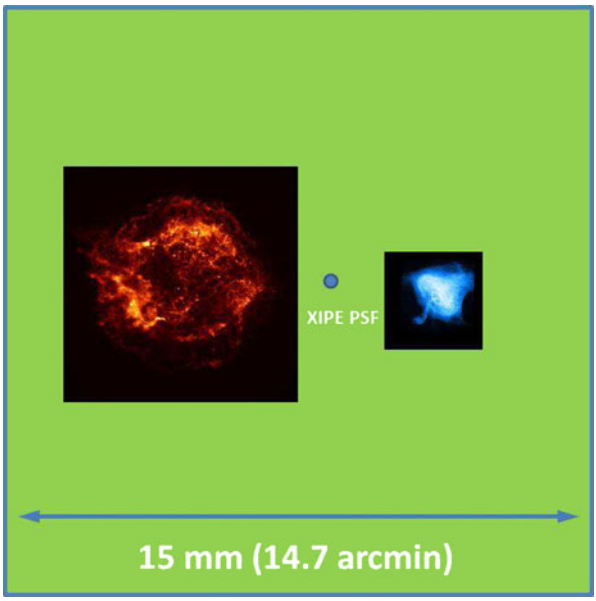

Fig. 1 The Chandra images of Cas A (*left*) and of the Crab Nebula (*right*) within the sensitive area of XIPE together with its PSF (Half Energy Width). The active area is 15 mm × 15 mm or 14.7 arcmin × 14.7 arcmin

fraction of the power-law component, polarization larger than 21 % (4-6 keV), 55 % (6–8 keV) and 70 % (8–10 keV), can be detected in each one of these subregions but interesting numbers could be obtained with just one energy integration for a significative measurement. Based on the Einstein survey [109]*, there are about ten SNRs with a small (< XIPE FoV) size having sufficient flux for X-ray polarimetry while the strategy for a space resolved measurement can be implemented after having analyzed the observation of Cas A. Oppositely large size SNRs* ($> 30'$) *with a clear X-ray synchrotron spectrum in their rims are SN 1006, RX J1713.7–3946, and RX J0852.0–4622.* Clearly all these considerations depend on how much the magnetic fields are ordered but this is precisely the scope of such measurements.

– **Pulsar wind nebulae** Spatially resolved X-ray polarimetry allows the magnetic field orientation in the torus, in the jet and at various distances from the pulsar to be determined. This makes it possible to evaluate the level of turbulence and instabilities exploring the acceleration mechanism responsible for the observed particle distribution [110, 134]. XIPE reaches an MDP of 2 % in 5 × 5 angularly resolved regions of the Crab Nebula in 10^5 s of observing time thanks to its imaging capability. The capability to resolve the surrounding nebula makes polarimetry of the pulsar more straightforward, allowing the emission model to be derived and compared for example with those studied in optical band [41]. A few additional PWNs will be accessible to XIPE for comparative measurements (see Fig. 1).
– **Jets** The acceleration mechanisms in jets and the related X-ray emission, especially at large distances from the central massive objects, for both galactic and extragalactic sources, is a very much debated issue and X-ray polarimetry can, in both cases, help to resolve the matter.

- $\mu QSOs$ The multiwavelength behavior of about two dozen X-ray binaries with relativistic radio emitting spots, superluminal for a few of them, indicates that they are a scaled-down version of radio-loud galaxies, with consequently much shorter characteristic variability timescales. By means of spectro-polarimetry in X-rays and at other wavelengths of these very luminous objects, it is possible to shed light on jet formation and evolution and their relation with the accretion disk emission. GRS1915+105, Cyg X−1, Cyg X−3, and XTEJ1550−564 have flux between one hundred millicrabs and several crabs, allowing an MDP < 1 %. They are also good candidates to search for General Relativity effects (see Section 3.2)
- *Blazars & Radiogalaxies* In Blazars, multiwavelength polarimetry, including X-rays, would allow for disentangling the origin of the second characteristic emission peak in their spectral energy distribution, thanks to a determination of the polarization angle. This peak is due either to synchrotron-self Compton (same angle as that of the synchrotron peak [15]) or to Inverse Compton (IC) of seed photons (different angle), presumably from the disk or from the broad-line regions. The degree of polarization of the IC peak allows the electron temperature [97] in the jet to be estimated. XIPE reaches an MDP of 3 % for Mrk 421 in 4×10^5 s.

  In some radio-loud AGN, the jet component can be as bright as the disk component in the 2–10 keV energy band, as in 3C273 [37, 38]. In this case, because the jet component is harder, a rotation of the polarization angle is expected.

- **Magnetic reconnection** Magnetic reconnection and subsequent acceleration of charged particles in the corona are at the base of the production of solar flares [12]. Actually, the Sun, providing a strong signal due to its closeness, acts as a Rosetta stone, clearly showing phenomena similar to those which may happen in objects significantly fainter and much farther away. Above 20 keV, see Fig. 2a (left), the emission from solar flares (Hard X-Ray, HXR) is mostly dominated by the non-thermal bremsstrahlung generated by high energy electrons impinging down on the chromosphere with a polarization degree as high as 40 % at 20 keV [147] (see Fig. 2b left and right, and its caption). Below 10 keV, the emission is mostly thermal due to plasma heating in the reconnection site and in the flaring loop filled with evaporated chromospheric plasma (see Fig. 2a, right). X-ray lines are present up to 7 keV [23, 93]. The thermal component is also expected to be polarized, although at a lower level than the non-thermal one, due to possible anisotropies in the electron distribution function [27]. Back-scattering further modifies the spectrum, especially at higher energies [4, 50]. X-ray polarimetry of the HXR offers the possibility to make a diagnostic of the level of the anisotropy of the electron beams, and of the magnetic field configuration, and to study the acceleration mechanism in the solar corona. Both RHESSI, with its spectrometer not designed to be a polarimeter [119], and the Thomson scattering polarimeter on-board Coronas-F [148] attempted to measure the X-ray polarization from

solar flares with only low significative results or large upper limits due to the high energy threshold of the former and to the high background/low efficiency of the latter. Moreover, future missions such as Solar Orbiter are not sensitive to polarization. XIPE performs polarimetry of radiation emitted by solar flares in the 15–35 keV energy band, reaching, for the two detector array configuration, an MDP of 0.6 % for an X10 class flare and 6.6 % for an M5.2 class flare. We estimated the sensitivity to different classes of solar flares using the spectra and the lightcurves in [105] in (1). We also evaluated the expected number of flares for each class, depending on the solar activity. Based on the forecast of the sun spots[1] we estimated that from July 2017 to June 2019 about two dozen flares are expected to be observed between class X10 and class M5. Being close to the solar minimum, the probability of an X flare is, however, small. XIPE solar polarimeter operates in an energy range where the spectrum of the flares is dominated by non-thermal bremsstrahlung but the flux expected is large. By measuring their polarization with good accuracy for a number of flares in different positions on the solar disk, it will be able to constrain different models (see Fig. 2b right and its caption) with much higher precision with respect to the data available today.

XIPE will also monitor the X-ray variability of the Sun between 1.2 and 15 keV with a small dedicated photometer with good energy resolution to determine the coronal average temperature and the related thermodynamic characteristics for either non-active or flaring corona. This also is particularly important for space weather studies.

2.2 Emission in strong magnetic fields

The presence of an intense magnetic field affects the propagation of the two X-ray polarization modes in a plasma. Moreover, it channels the plasma along the field lines, causing an asphericity in its distribution. Both phenomena produce radiation which is observed as anisotropic and polarized.

- **Accreting white dwarfs** In White Dwarfs (WDs) with a strong magnetic field, X-ray polarization derives from the scattering on the WD surface, from its accreting column and, when present, from the (truncated) disk. The polarization signal is periodic and energy dependent, with values ranging from 4 % to 8 % [66, 70]. XIPE can search for phase-dependent X-ray polarization in the brightest objects. For AM Her, XIPE reaches an MDP of 6 % in each of ten phase bins with 10^6 s of observation.
- **Millisecond x-ray pulsars** Accretion is responsible for the spin-up of neutron stars up to the maximum possible rotation speed. Compton scattering in the accretion shock, which is localized and not extended as shown by pulsation,

[1] http://www.swpc.noaa.gov/ftpdir/weekly/Predict.txt, 2012/04/04

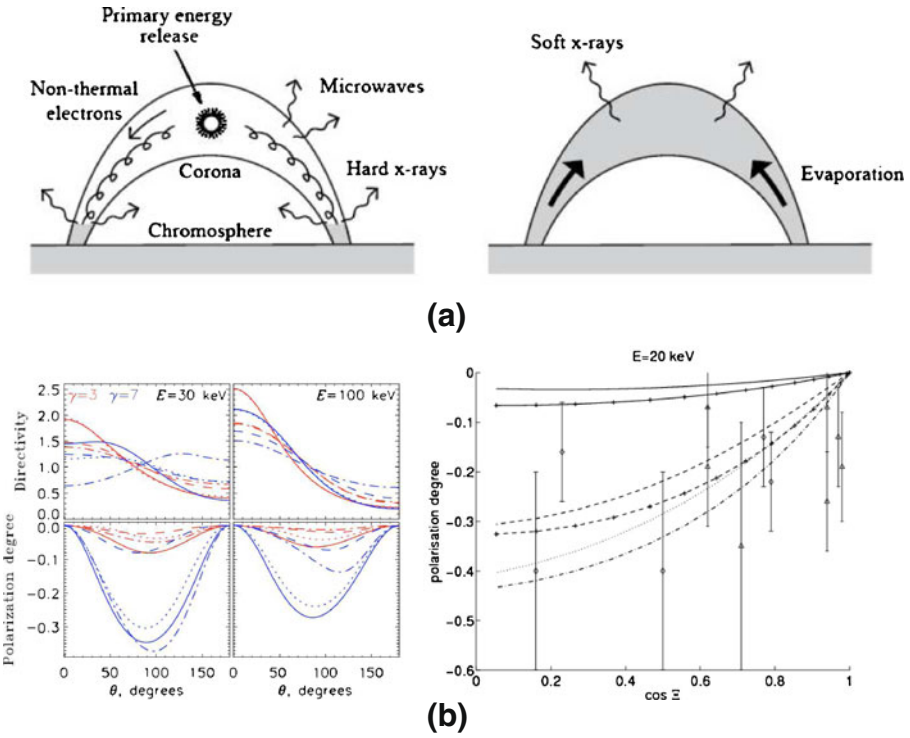

Fig. 2 **a** Sketch of the flaring loop in hard X-rays and soft X-rays (figure from [101]) **b** (left) Directivity and polarization degree *resulting from the integration over all the coronal magnetic tube*. The directivity is the ratio between the intensity at a given angle and the average intensity (unit value means isotropic emission). The model explores two initial different power-law indices of the particles that are accelerated: $\gamma = 3$ (*red lines*) and $\gamma = 7$ (*blue lines*). Different lines show different models for the simulation: *solid lines*: pure collisions(C), *dashed line*: collisions and converging magnetic field (C+B), *dotted line*: collisions and return current (C+E), *dash-dotted line*: all factors are taken into account (C+E+B). θ is the radiation propagation direction that is the angle between the normal to the sun where the injection and the downward beaming occur and the observer. A higher polarization is expected when θ is 90° therefore when the flare is located on the limb. (**b** (right)). Comparison of the polarization expected from different models with available data at 20 keV as a function of Ξ that is the position angle in the solar disk ($\cos(\Xi) = 1$ is the disk center and 0 is the limb) for an electron beam with wide angle dispersion ($\Delta\mu = 0.2$ where μ is the cosine of the pitch angle of the precipitating electrons). The electrons' energy flux is 10^{10} erg cm$^{-2}s^{-1}$. For $\gamma = 3$ the following models are shown: solid line C+E model, solid line with crosses: C+E+B model. For $\gamma = 7$ the models are: dashed line C+E model, dashed line with crosses C+E+B model. The cases of a more collimated electron beam ($\Delta\mu = 0.09$ with $\gamma = 7$ and C+E model) are also shown. The initial electron energy fluxes are respectively (10^{10} erg cm$^{-2}s^{-1}$) (*dot-dashed lines*) and 10^{12} erg cm^{-2} (*dotted lines*). The data are from [124–126] (at 15 keV, diamonds) and from [129] (16–21 keV, triangles). The figures are from [147]

polarizes the radiation at higher energies [132]. Phase resolved X-ray polarimetry allows for testing this model and, possibly, for discriminating an alternative scenario where the scattering is from the accretion disk [107]. It also provides the geometrical parameters, such as the orbital and magnetic inclination, which

are usually free parameters in the evaluation of the mass and the radius of the neutron star. At the present time 14 accreting millisecond X-ray pulsars (AMXP) are known and they are very faint in quiescence. They, however, can serendipitously outburst for several days with fluxes exceeding tens of milliCrabs and more, showing their kilo-Hz pulsation. At a flux of 10 m Crab, rather low for this kind of sources, and integrating for 10^6 s, e.g. SAX J1808-4-3658 reaches an MDP of 3 % in 5 phase bins that is sufficient for modelling the source.

– **Accreting x-ray pulsars** In accreting X-ray pulsars, the large magnetic field (10^{12}–10^{13} Gauss) derived from the observed cyclotron lines creates birefringence effects with an energy and phase dependent polarization signature [72]. Phase resolved X-ray polarimetry allows for determining the geometry of the accretion (*fan* or *pencil* beam), the position of the rotation axis in the sky and the angle between its position and the magnetic dipole. Many X-ray pulsars can be observed by XIPE with sufficient sensitivity. For example, an observation of Her X-1 is characterized by an MDP of 3.5 % in 10 independent phase bins.

2.3 Scattering in aspherical situations

– **X-ray binaries** The 2–10 keV spectrum of accretion-disc-fed X-ray binaries in the hard state is probably mostly due to Comptonization by a hot corona. The aspherical geometry produces polarized X-rays [40, 98, 99] and the polarization degree places constraints on the unknown geometry of the hot corona [108]. Above 7 keV, the Compton reflection of the primary emission from the disk is also expected to be polarized with a polarization degree that depends on the disk inclination and on the anisotropy of the intrinsic emission [67, 100].
– **Radio-quiet AGNs** In radio-quiet AGNs, the Comptonization in the corona and the Compton reflection from the disk always dominate with respect to the disk emission mostly irradiating in UV or in soft X-ray, and the same considerations as above apply [108]. A XIPE observation of IC4329A of 3×10^5 s yields an MDP of 3.6 %. In addition to the above reflection environments, scattering can occur in AGNs on the so-called molecular torus, whose geometry is still largely unknown, and on the ionization cones when present (see Fig. 3). X-ray polarimetry (see Fig. 3b) can shed light on the connection between these two regions as well as on the true torus geometry [34]. In the case of NGC 1068, an MDP of 4.2 % can be reached with an observation lasting 5×10^5 s. With an observing time of 10^6 s the 3-σ measurement is at level of 5 % (2–4 keV) and 6.9 % (4–10 keV). With this sensitivity it is possible to disentangle most of the models and to provide an additional 1-σ error on the angle of 9.5° (see paragraph 4) that is sufficient to hint the possible rotation of 60°. A multiwavelength polarization campaign can allow for a deeper investigation of the geometries of the scattering regions [34, 64] in AGNs.
– **X-ray reflection nebulae** There are a few molecular clouds in the Galactic Center region whose X-ray spectra are well reproduced by a pure Compton Reflection component, indicating that such clouds are reflecting the X-ray radiation produced by a source outside the cloud. The most famous example is Sgr B2,

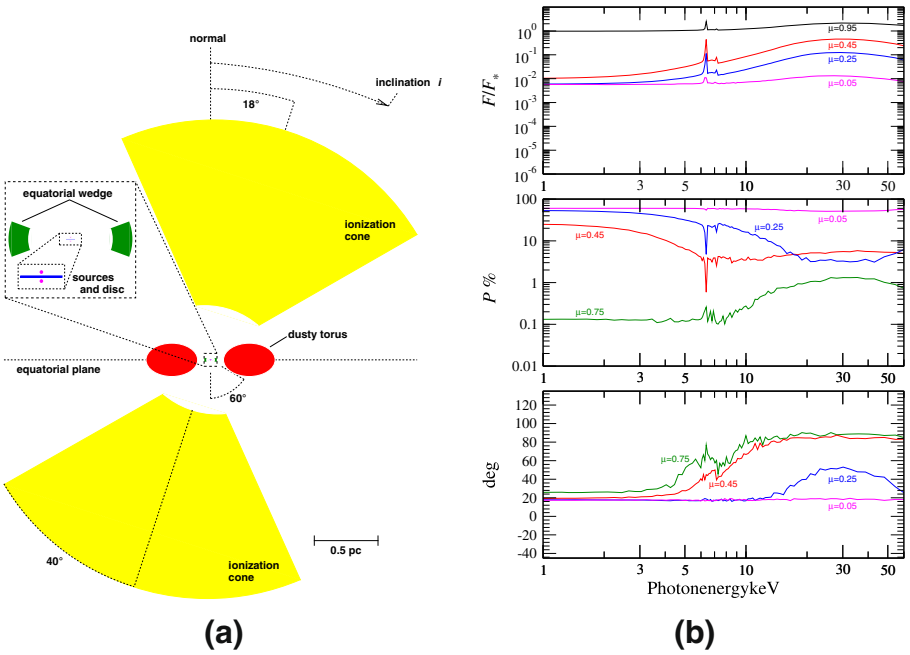

Fig. 3 **a** Sketch of the scattering environment around NGC 1068. **b** Intensity, level of polarization and polarization angle as a function of energy for the model of Fig. 3a. Here the column density of the torus is $N_H = 10^{27}$ cm^{-2} and the optical depth of the scattering cones is $\tau_{cone} = 0.3$. $\mu = \cos(i)$ where i is the viewing direction measured with respect to the disk and torus symmetry axis; $F_\star$ is the total flux of the primary source, emitted into the same viewing direction. Both figures are from [34]

but more recently, the X-ray emission from the Sgr C complex was additionally proposed to have the same origin [85]. The puzzle here is that there is no X-ray source bright enough in the surroundings. It has been proposed, therefore, that these clouds are reflecting past emission from the central black hole [56, 120], which should have undergone a phase of strong activity about three hundred years ago. If the emission from the nebulae is indeed due to scattering, it should be very highly polarized [16], with a direction of polarization normal to the scattering plane, and therefore to the line connecting the cloud to the illuminating source. The detection of polarized X-ray emission from one or more of these clouds would place a strong limit on the position of the source which illuminated them in the past and, if the polarization plane is indeed perpendicular to the direction towards Sgr A*, it will be proved that not many years ago the Galaxy was a low luminosity AGN. In addition, measurements of the polarization degree will provide unique information on the position of the clouds with respect to Sgr A* along our line of sight. The flux from Sgr B2 is evolving with time. It is currently decreasing [57], probably reflecting the evolution of the illuminating source flux in the past. Other reflecting nebulae are present around the central black hole, which are also varying with time, e.g. Sgr C [83, 85], and

the brightest of them when XIPE will be in orbit will of course be chosen for observation. Although it is not possible to estimate the flux of Sgr B2 when XIPE will be in orbit, assuming the flux measured by *BeppoSAX* [111] and a polarization of 40 %, the precision with which the polarization angle can be measured in 2×10^6 s is 3.5° (1-σ), good enough to set tight constraints on the origin of the illuminating radiation. One question is the background rate expected when observing this very faint extended X-ray source. This question is answered in Section 5.1.2. Here we just write that the background is still about 30 times smaller with respect to the expected source rate as based on estimates from [13]. The image of Sgr B2 on the detector active area is shown in the collage of Fig. 4.

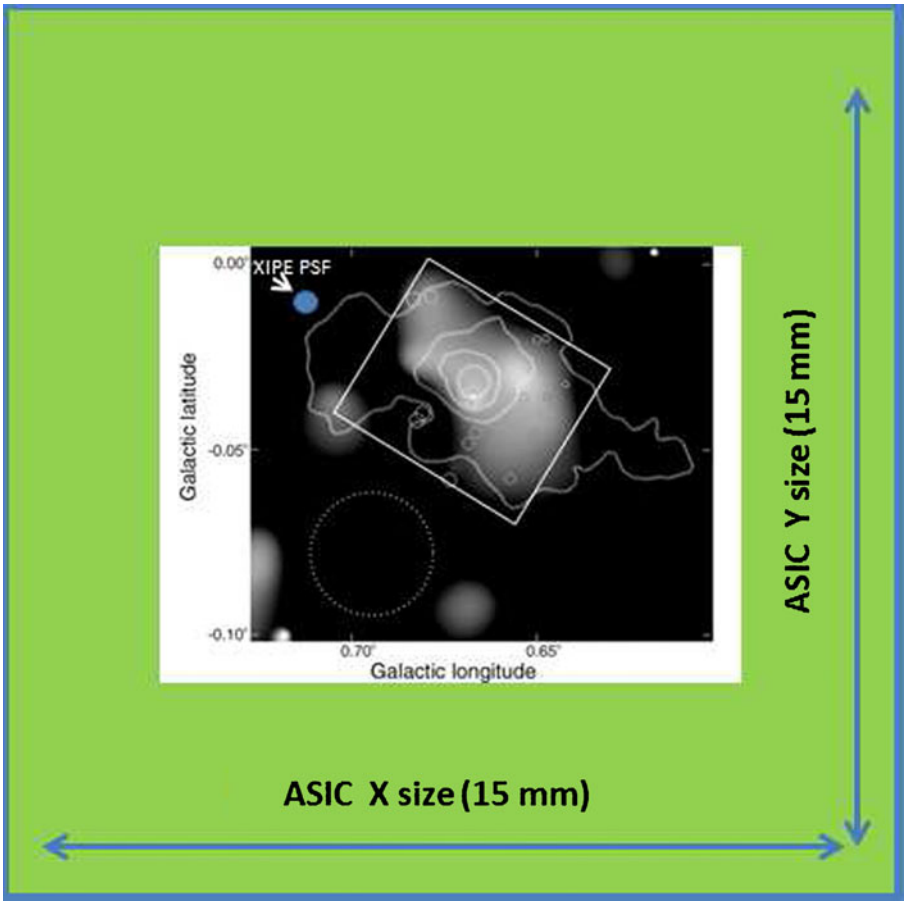

Fig. 4 Image of Sgr B2 on the GPD active area as in [84]. For XIPE, we assume half of this region where we evaluated the background. The green area represents the total active area of the X-ray polarimeter. The galactic coordinates shown are in degrees. The active area is 15 mm × 15 mm or 14.7 arcmin × 14.7 arcmin. The XIPE PSF is the Half Energy Width

3 Fundamental physics with XIPE

High Energy Astrophysics makes accessible natural laboratories of fundamental physics, providing tests of physical theories which would otherwise be impossible. X-ray polarimetry is a sensitive probe because distinctive signatures on the degree and angle of polarization are expected during photon transfer in strong gravitational or magnetic fields. Energy dependent rotations of the polarization angle and variations of the polarization degree from distant sources may reveal Quantum Gravity effects and allow for axion–like particle searches.

3.1 QED in strong magnetic fields

Emission from a neutron star (NS) surface is expected to be polarized because the opacity of the atmosphere to photons polarized perpendicular to the magnetic field (X-mode) is smaller than that for parallel polarized radiation (O-mode) [89]. The radiation in the X-mode can escape from inner (and, therefore, hotter and brighter) layers of the NS atmosphere. The expected degree of polarization induced by this effect is not large, at level of 5–25 % [90], because of the different magnetic field orientations at the emission sites. Although this basic result is commonly accepted, the detailed photon transfer across the atmosphere is strongly affected by quantum-electrodynamics (QED) effects because a magnetic field in excess of 10^{14} Gauss for magnetars polarizes the vacuum [71]. As discussed in Section 3.1.1 and in 3.1.2, QED produces three detectable effects on X-ray polarization. One effect is on the energy dependence of X-ray polarization degree and angle, due to the presence of a vacuum resonance. The other two effects are the enhancement of the maximum degree of polarization and the observable lag of the polarization angle between optical light and X-rays, both due to birefringence. The signatures on the spectrum (softening of the hard tail and reduction of the equivalent width of the proton-cyclotron line) can be less evident and, at the same time, the modelling is affected by the degeneracy on the various parameters. Polarization measurements can be used to disentangle these degeneracies [131].

3.1.1 The effect of the vacuum resonance

Detailed calculations [31, 130] have shown that QED effects have a peculiar signatures on the polarization of the radiation detected by a distant observer, while they have a less obvious impact on spectral parameters. A resonance, occurring when the contribution to dielectric tensor of the plasma and of the vacuum compensate each other, should produce a transition between the two photon modes analogous to the Mikheyev-Smirnov-Wolfenstein mechanism for neutrino oscillation [59]. The probability of a transition between the photon modes depends on the geometry, magnetic field, and properties of the medium, increasing monotonically with the energy of the photon. For the magnetic field regime $B < 7 \times 10^{13}$ Gauss, the resonance typically lies outside the photospheres of the two photon modes. Since surface emission is usually dominated by the X-mode, at energies $\gtrsim$ a few keV, X-mode photons are converted to O-mode photons after decoupling from the atmosphere, leading to

a rapid 90° shift in the angle of polarization. For stronger, magnetar-strength magnetic fields, the resonance occurs inside the O-mode photosphere; thus, the rapid rotation in the plane of polarization does not occur (see Fig. 5). Detecting the 90° rotation in normal pulsars but not magnetars would independently confirm the presence of super-strong magnetic fields in magnetars. Such rotation can be excluded for example in the case of SGR 1806-20 a bright (not the brightest) magnetar. In 10^6 seconds we can get a 3-σ measurement at level of 23.6 % (2–4 keV) and 21.3 % in (4–10 keV) for each of the 5 phase bins. This level of polarization, well below the expected value from the model of [31] showed in the Fig. 5, implies a 1-σ error in angle of 9.5°, a precision that is sufficient to exclude the 90° rotation in the data.

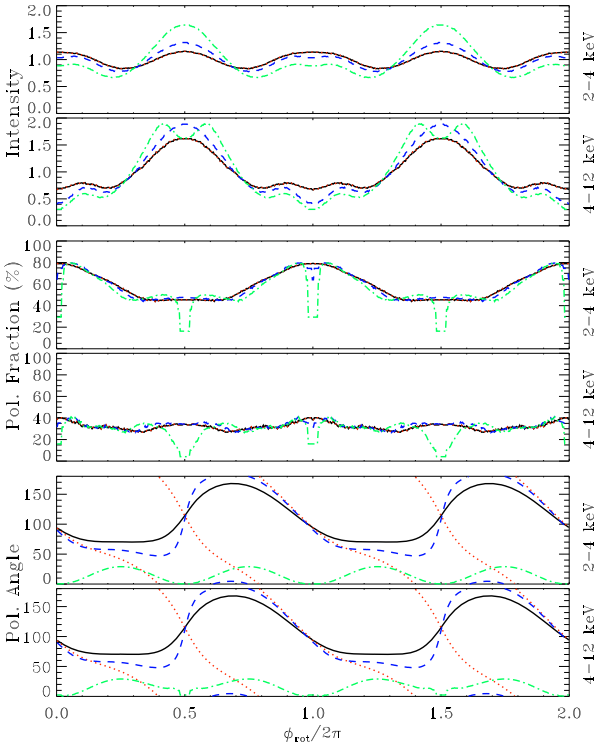

Fig. 5 This figure (from [31]) is the result of a Monte Carlo simulation of the phase-resolved emission observed from a magnetar with an arbitrary flux modelled as *t12g18c90Eu* ($\Delta\phi$NS(rad)=1.2, γmax = 1.8, seed pol=E-mode, $\Theta_{cap}(^\circ) = 90$, where $\Delta\phi$ is the twist angle of its magnetosphere, γ max is the maximum Lorentz factor of the electrons in the magnetosphere, Θ_{cap} is the angular size of the emitting polar cap). From top to bottom are shown the intensity, the polarization fraction and the polarization angle as a function of rotational phase (two full periods shown) in energy bands (2–4 keV and 4–12 keV). The pair of angles (θ_{rot} the angle between the magnetic axis and the rotation axis, θ_{los} the line of sight from the rotation axis) of (45°, 70°) is represented by a *solid/black line*, (70°, 45°) is dotted/red, (60°, 70°) is *dashed/blue* and (90°, 90°) is dot-dashed/green. It can be seen that the polarizations in the two energy bands are always in phase

3.1.2 The effect of birefringence

X-ray polarimetry of NS emission provides an opportunity to observe another QED effect: vacuum birefringence induced by a strong magnetic field. This effect was predicted nearly 70 years ago [42, 140] but still needs to be verified experimentally. If the vacuum birefringence is present, the indices of refraction of the two linear polarization modes differ from each other. Vacuum polarization produced by a NS magnetic field is indeed sufficient to decouple the polarization modes, so that the direction of polarization follows the direction of the local magnetic field [43]. When modes are coupled again at a distance which is large with respect to the radius of the NS, the local magnetic field is almost parallel and therefore photons coming from different regions of the NS surface add coherently. This produces a 5–7 times larger polarization degree in the NS phase averaged signal [44] than in estimates where birefringence is not taken into account [90].

In addition, the NS and its magnetosphere rotate and, since the modes of lower energy radiation couple first, another observable prediction of the presence of vacuum birefringence effects is that the angle of polarization at low energy should lag behind higher energy photons [43]. For the Crab pulsar, the lag between X-rays and optical emission should be about 10 degrees, as derived in the Deutsch model [22] in [43].

3.2 General relativity in extreme gravity fields

The emission from the accretion disk is the brightest component of the X-ray spectrum from Galactic Black Holes when they are in a high state. The strong gravitational field in the innermost region of the disk, that is responsible for the X-ray emission, causes a rotation in the polarization angle larger than for a rotating black-hole and for higher energies [18, 24, 58, 62, 108, 116]. The measurement of the rotation of the polarization angle (and degree) with energy, and therefore of the spin of the black-hole, allows for testing General Relativity in extreme gravity fields. The best but not the only source to search for this effect is GRS1915+105 (see Fig. 6), a bright μQSO whose 2–10 keV emission is, when in high state, dominated by thermal emission. Moreover, the source is highly inclined (70° in [75]), and therefore the polarization degree is expected to be high. Other less inclined sources may show lower polarization levels, which could still, however, be easily detected in several other bright objects. In addition, about 4 transient BH binaries are expected to have a large enough flux to be measured during 2 years of operation and they are good sources to search for GR effects.

In AGNs, the thermal emission from the disk peaks in UV and therefore lies outside the energy band of XIPE. Strong Gravity effects manifest themselves with the temporal variation of the polarization angle from reflected X-rays [25] from a primary source with changing height from the accretion disk (see [74]), as in the case of MCG–6–30–15. In this source, an MDP of about 4 % can be reached in 300 ks. A long look (1 Ms or more) at this source may provide a first test of the model. Alternatively, there is at least one galactic black hole candidate (XTE J1650–500) which is thought to behave like MCG–6–30–15 on a smaller scale [102, 104]. Thanks to a factor of 100 higher flux, this source would allow for deeper studies of this phenomenon.

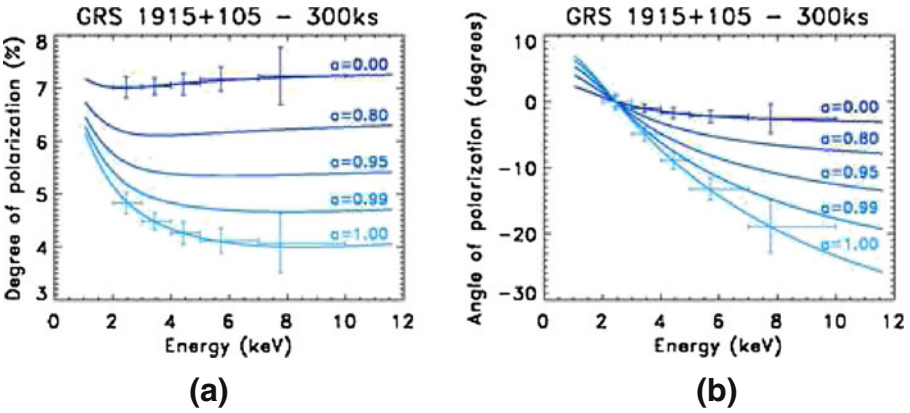

Fig. 6 **a** Expected variation of the polarization degree with energy in GRS1915+105 simulating an observation of 300 ksec (The model is from [24] while the errors are evaluated for the case of an observation with XIPE). **b** Polarization angle rotation with energy in the same observation

An alternative model explains the observed relativistic iron line from MCG–6–30–15 as a non-relativistic feature arising from partial covering [73]. Partial absorption in a clumpy outflow intercepting the line of sight generally induces low-polarized forward scattering and always produces a polarization position angle that is constant in energy. In the reflection case, on the other hand, the polarization is larger and its position angle varies systematically with energy. A larger polarization is expected at higher energies and a long-look observation of 2 Ms can detect polarization above 3 % (4–10 keV) as expected by the the reflection model [65] only, and thus strongly favor one of the two interpretations, see Fig. 7. Furthermore, [46] pointed out two

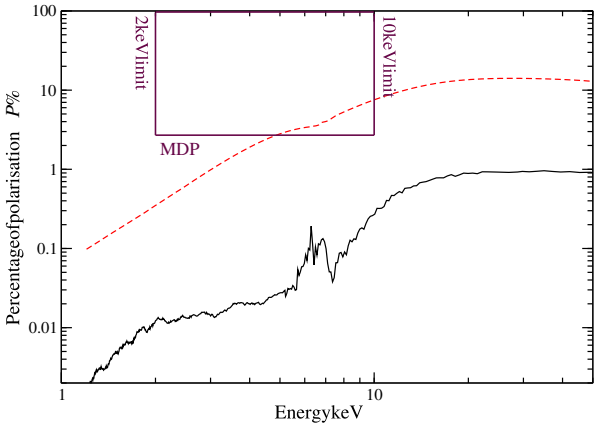

Fig. 7 MDP of the two scenarios for a 1 Ms observation of MCG–6–30–15. The solid curve represents clumpy absorption, while the red dashed curve is relativistic reflection induced by a Kerr super massive black hole with spin parameter $a = 1$. With an observation of 2 Ms a polarization larger than 3 % (MDP) can be detected between 4 and 10 keV to be compared with a higher (3.6 %) expected average polarization degree, after spectral convolution in the same energy band. The figure is from [65]

specific effects of general relativity that can be revealed in linear polarization from light scattered by relativistic jets that are expected due to indirect photons passing in the immediate vicinity of a black hole.

3.3 Quantum gravity

The identification of a good candidate observational test for studying Quantum Gravity in its different forms (loop, string, non-commutative space-times) is presently still a challenge [1]. Polarimetry is one of the few possible probes [32] of loop Quantum Gravity. At the quantum scale, birefringence would be responsible for a rotation of the polarization angle along the photon path. Such rotation, in the linear case, is proportional to the source distance and to the square of the energy by means of a dimensionless factor η [76]. The scale of breakdown of the usual dispersion relation is $\eta = 1$, the Plank scale (see for example [30]). Detecting a non-vanishing linear polarization from distant sources allows upper stringent limits to be placed on η, and cases other than linear to be excluded. Upper limits based on these observational tests already rely on the UV polarization of a radio galaxy [33] and on X-ray polarization of the Crab Nebula measured by OSO–8 as in [51] ($\eta < 10^{-4}$). A more stringent upper limit comes from the UV/optical polarization of Gamma-ray burst afterglows as in [30] ($\eta < 10^{-7}$). In hard X-rays, upper limits from INTEGRAL data (see, for example, [60, 63, 117]) are instead based on results derived from the prompt emission of Gamma Ray Bursts [54, 69] and from the Crab emission [21]. Such low-significance results are still debated. Sometimes, different instruments on-board are themselves in contradiction. We stress that the detectors were not primarily designed as polarimeters. Such instruments were never calibrated on-ground or in-orbit for this purpose. In this regard [127] noted that the data in the measured modulation curves in [69] are not distributed with Poissonian statistics (while this is assumed in the evaluation of the error contours for example in [21]). Recently, by using the measurement ($P = 84^{+16}_{-28}$, 3.3 σ significance) for GRB 110721A, with a known redshift of 0.382 (see [143] and reference therein) by the GAP GRB Compton polarimeter aboard IKARUS, an upper limit $\eta < 10^{-15}$ was evaluated in [127]. Looking to different sources at different distances the relation between the latter and the rotation of the polarization angle with energy can be tested with respect to a possible intrinsic polarization angle variability. With an observation of 10^6 s, values of η down to 3×10^{-10} can be reached with XIPE using e.g. the known Blazar 1ES1101–232, at $z = 0.186$, with a clear synchrotron spectrum and high optical polarization, assuming it has a 10 % polarization degree in the X-ray band. By performing polarization measurements from several bright enough Blazars at different distances, observed to pursue other scientific objectives, XIPE can put the results on a firm statistical basis (as discussed for GRBs in [55]).

3.4 Search for axion-like particles

Axion-like particles (ALP) are bosons that are predicted in extensions of the Standard Model. They can form the so-called cold dark matter responsible for the formation of structures in the Universe and, conversely, be the quintessential dark energy

responsible for the acceleration in the cosmic expansion. Axions mix with photons in the presence of a magnetic field with a rotation of the photon polarization and possibly with the production of elliptical polarization from linear.

Such an effect was searched on-ground by Polarizzazione del Vuoto con LASer (PVLAS), a dedicated experiment with initially positive results but successively withdrawn [144, 145]. PVLAS has recently been upgraded [146].

On-ground experiments are limited by having short baselines and the consequently small effects on polarization. Searching for this effect in distant astrophysical sources overcomes this limitation. This effect may be detectable in neutron star atmosphere spectra; however, because photon-axion conversion occurs only for the O-mode, this signature is much easier to detect using polarization measurements than standard spectroscopy [94].

Other authors [5, 91] suggested that in case of a very light ALP, photon-ALP mixing in intergalactic, intracluster and Galactic magnetic fields may significantly affect the polarization of radiation emitted by distant sources, inducing either a linear polarization on initially unpolarized photons or a dispersion of the degree of polarization of initially linearly polarized ones (see Fig. 8). Clusters of galaxies emitting in X-rays, and a dozen with a flux large enough for polarimetry, are expected to have very small or null linear polarization in origin. A detection of a large polarization from clusters could be the signature of photon-ALP mixing (see for example lower-right panel of Fig. 8). Moreover imaging allows the contribution of possible AGNs or of foreground objects in the FoV to be excluded.

Moreover, ALP signatures should strongly depend on energy and on the projected position of the object on the sky because of the difference in magnetic field morphology in different directions of observation. Natural candidates for these studies are again Blazars where ALP-induced effects can be searched but also the correlation between the polarization of galactic sources and the viewing direction. A sample of Blazars with the synchrotron peak emitting in X-rays, if the photon-ALP mixing is acting, should show an X-ray polarization distribution larger with respect to the corresponding distribution in optical wavelength, due to the presence of a cut-off energy for this effect, in a way that depends on the distance.

4 Science requirements for a small imaging X-ray polarimetry mission

The capability to measure the degree of polarization and the angle of polarization can be expressed in terms of the MDP that represents, at a certain confidence level, the level of the signal which can be attributed solely to statistical fluctuations in the instrumental response. In fact, polarization is a positive-definite quantity and therefore it is always measured to some extent. Only a detection greater than the MDP is statistically significant, and to reach a 3-σ measurement of a particular level of polarization, an integration time 2.25 longer than that corresponding to the same MDP is required in case, as it is common practice in X-ray polarimetry, both the angle and the modulation amplitude are simultaneously measured [26, 118, 139]. A measurement at 3-σ of the polarization degree allows a 1-σ confidence interval on the position angle of about 9.5° to be reached [26, 118]. If the level of background is

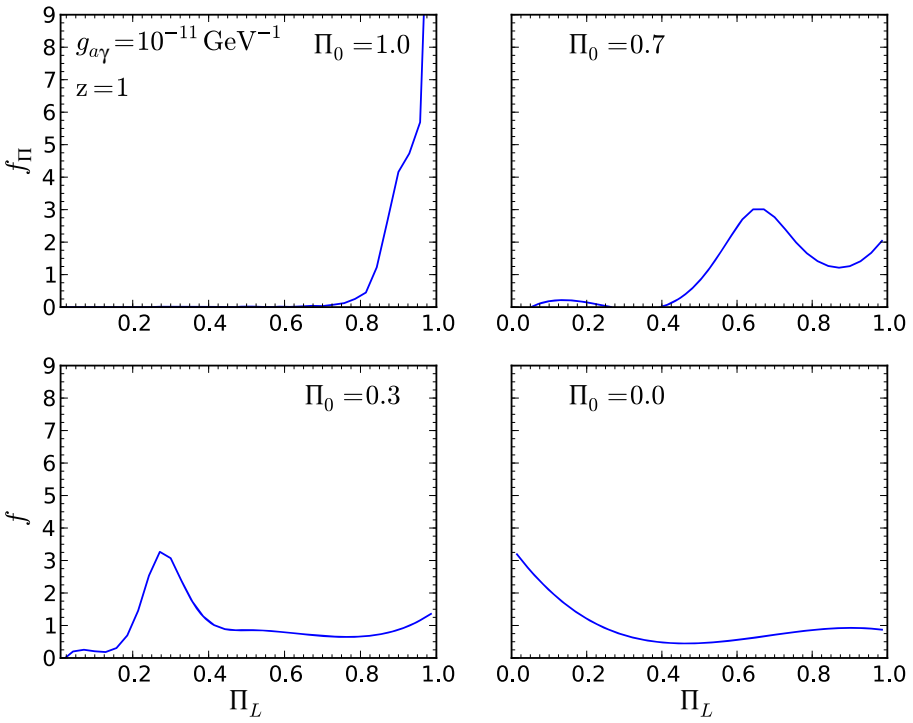

Fig. 8 Probability density function derived by simulating the propagation of X-rays in the extragalactic magnetic field and the photon-ALP coupling. It is shown the final polarization measured for initially linearly polarized photons emitted at $z = 0.3$ from GRBs or other distance sources. The sources have an initial fixed polarization of 100 %, 70 %, 30 % or 0 %. The magnetic field coherent length scaling and the plasma density used corresponds to the Wilkinson Microwave Anisotropy Probe (WMAP) constraints. The figure is from [5]

negligible with respect to the counts from the source, the MDP at 99 % confidence level is expressed as:

$$MDP = \frac{4.29}{\mu\sqrt{S}\sqrt{T}}. \tag{1}$$

In (1) μ is the so-called modulation factor, S is the source counting rate and T is the observing time. The requirement on the imaging capability is important for two reasons: first of all, imaging is necessary to single out the target source from others in the *FoV*, thereby reducing the underlying background. Moreover, imaging is a powerful tool for performing angularly resolved polarimetry of extended sources (e.g. Pulsar Wind Nebulae, Supernova Remnants). Since it is expected that only one solar flare will occur at a time and that it is usually much brighter than the background, scientific objectives on solar physics do not pose any imaging requirement.

A moderate energy resolution is required to perform energy-resolved polarimetry of source continua and to disentangle the dependency on energy of the instrumental response, e.g. the modulation factor and the efficiency.

XIPE scientific requirements on the timing resolution and timing accuracy are driven mainly by the necessity to resolve in phase the emission of rapidly spinning millisecond pulsars. The timing requirement for the solar flares polarimeter is less stringent, except for the dead time.

The pointing accuracy is defined to include in the *FoV* extended sources such as the Crab Nebula. The range of duration of an observation that spans from a few kiloseconds to one week is requested to arrive at the required sensitivity. However, a set of on-board calibration sources must be provided to check the performance stability.

The short duration of the mission implies no particular requirements on the stability performance since the XIPE payload is already built with space-proven technology typical of X-ray Low Earth Orbit instrumentation.

5 The payload

XIPE has four instrument units, two identical Efficient X-ray Photoelectric Polarimeters (*EXPs*), a Medium Energy Solar Polarimeter (*MESP*) and a Solar Photometer in X-rays (*SphinX*) described in the following paragraphs.

The two EXPs comprise two identical pairs of X-ray telescopes and focal plane instrumentation. The X-ray telescopes are a heritage of the JET-X project, for which four mirror modules (MMs) were developed, as well as three flight model units (FM) and an *Engineering Qualification Model* (EQM) used for the qualification test campaign but with the same characteristics of the 3 FM units.

5.1 The astronomical X-ray polarimeter

As already mentioned, the XIPE payload is a descendant of POLARIX [20] but with only two telescopes, to be compliant with the resources of an ESA small mission. The Gas Pixel Detector (GPD) is, however, evolved in a configuration (see Fig. 9b) with a larger cross section.

5.1.1 The detector and the mirrors

The GPD [9] is a gas cell made of MACOR filled with a mixture of 20 % He and 80 % DME, with a thin 50 μm Beryllium entrance window glued on a titanium frame, a drift gap (1 cm), a charge amplification stage and a multi-anode read-out. X-rays absorbed by the gas are converted into ejected photoelectrons that in turn produce an ionization pattern in the gas. The track is drifted by a uniform electric field to the Gas Electron Multiplier (GEM), and there the charge is multiplied with a negligible change in the shape.

Below the GEM, at a distance of less than a few hundred μm, the top layer of a multilayer ASIC (Application Specific Integrated Circuit) CMOS (Complementary MetalOxide Semiconductor), is covered with 105600 metal hexagonal pads with 50 μm pitch and a high filling factor. The ASIC CMOS [8] chip is glued and internally bonded to a Kyocera alumina package whose pins are externally soldered to

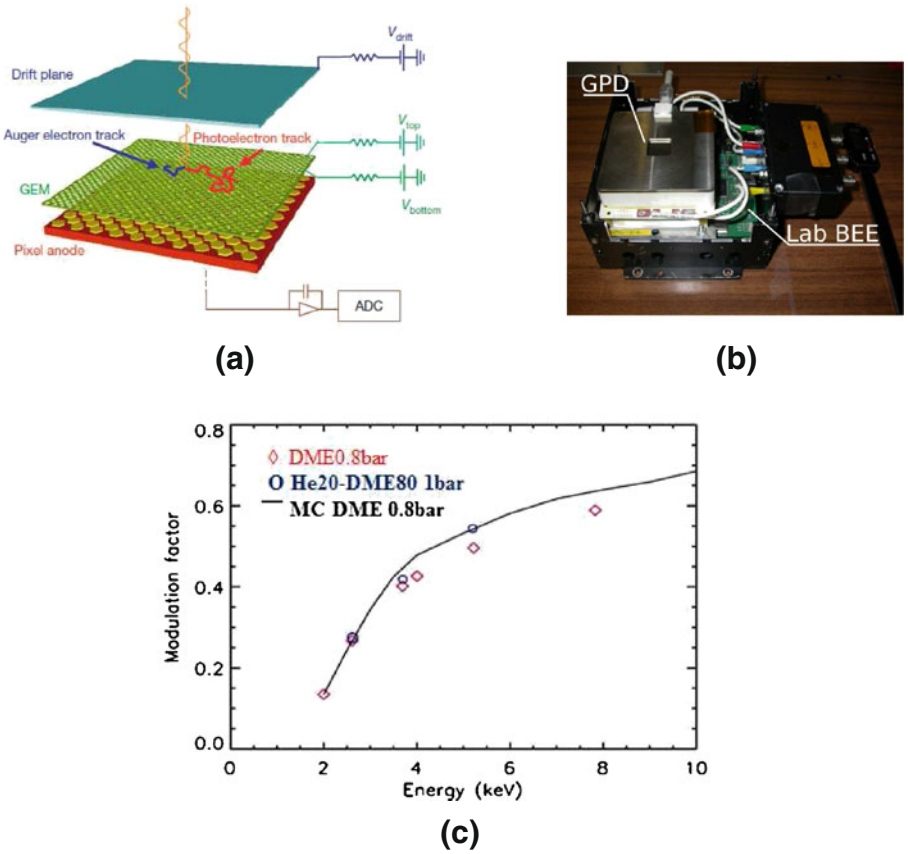

Fig. 9 **a** The sketch of the different components of the GPD. **b** The current GPD prototype having a larger body, but the same active area, with respect to the first sealed version [9] with a more uniform electric field and background. BEE is the laboratory back-end prototype. The flight BEE is described in Paragraph 5.3. **c** The measured modulation factor for two filling mixtures, at different energies, compared to Monte Carlo simulation

a Printed Circuit Board. The bottom layers of the ASIC CMOS constitute complete readout electronics independent for each pixel. The self-triggering capability is coupled to the selection capability of the sub-frame containing the photoelectron track. The image of the latter is analyzed by an algorithm [7, 88] that provides the impact point with a resolution of 30 μm rms [114] and an estimate of the emission direction. Photoelectrons derived from polarized photons have emission azimuthal directions distributed as $\cos^2(\phi)$, where ϕ is the angle with respect to the polarization vector.

While generating the so-called modulation curve, the degree and the angle of the linear polarization of the incoming photons are derived from the amplitude and phase.

The mirror modules were developed at the Brera Observatory and manufactured by Medialario with an electroforming replica process. They consist of 12 gold coated Nickel shells with a Wolter I geometry, with diameters going from 191 to 300 mm and a total length os 600 mm. The focal length is 3500 mm. They have been calibrated

many times at the PANTER X-ray test facility for a variety of energies and off-axis angles. The total effective area of a single unit for some energies of interest is reported in Table 3.

The Half Energy Width (HEW) is ∼15 arcsec at 1.5 keV and ∼19 arcsec at 8 keV [141]. At the end of November 2012, as described in Section 6, the JET-X (FM 2) optics was again calibrated at PANTER X-ray test facility. Preliminary results show [115] that the effective area and the angular resolution are presently basically preserved, and, therefore, the optics are still suitable for an X-ray experiment with good imaging capabilities. The total mass of each (MM) unit is of 59.9 kg and the maximum diameter of one mirror unit is at the interface flange, and this corresponds to a diameter of 388 mm. A maximum gradient of less than 2 °C assures that the HEW is not degraded by more than 10 arcsec.

JET-X optics have been already qualified for a launch with Proton rockets (for the JET-X experiments on-board Spectrum-X-Gamma) and DELTA rockets (for the Swift mission). The EQM module can be used for the qualification with other launchers (e.g. Vega). The effective area of the JET-X optics and the efficiency make the GPD sensitive in the energy range of 2–10 keV.

The sensitivity achieved with this configuration [80] is already compliant with the scientific requirements. However, a continuous search in the parameter space of gas thicknesses and mixtures is being conducted with the intention of arriving at an even better figure of merit (i.e. to optimize the parameters of the gas mixture, such as the electron transverse diffusion, the scattering probability and the charge gain).

A prototype GPD was thermo-vacuum tested between −15 °C and +45 °C and irradiated with a Fe ion dose corresponding to several years in orbit [6]. GEMs produced with the current technology have been successfully irradiated with protons and heavy ions [48]. The main characteristics of the EXPs GPD on-board XIPE are summarized in Table 1.

Table 1 Characteristics of EXP and MESP on-board XIPE

Parameter	2 × EXP units (2 × MESP units)
Polarization sensitivity	MDP = 14 % in 100 ks for 1 mCrab
	0.6 % for an X10 flare; 6.6 % for an X5.2 flare (MESP, 15-35 keV)
Imaging capability	24 arcsec (HEW, *overall*), 14.7 × 14.7 $arcmin^2$ FoV
Spectral resolution	20 % @ 5.9 keV
Timing	Resolution: 8 μs; Accuracy: 2 μs; Dead time: 10 μs (negligible)
Gas mixture	20 % He-80 % DME 1-atm 1-cm (EXP)
	60 % Ar-40 % DME 3-atm 3-cm (MESP)
Energy range	2–10 keV (EXP)
	15–35 keV (MESP)
Background	EXP: 5.5 × 10^{-7} c/s (4.8 nCrab, point source) [113]
	MESP: negligible for solar flare X-ray polarimetry

It should be noted that the scientific requirements for XIPE are fulfilled even with a payload hosting a single GPD and a single telescope. Two telescopes allow the same sensitivity to be obtained in half of the time, making possible larger population studies in the time frame of the mission.

5.1.2 The background of XIPE

The residual background of the GPD is not, at the present stage of development, minimized by means of the use, for example, of an anti-coincidence system or pulse shape discrimination as in the case of a traditional gas multiwire proportional counter. However, all these methods exploit in some way the space distribution of the charges produced by the detection event. The same and possibly better can be done with the GPD that resolves the track. The high granularity of the detector surface and simple methods of pattern recognition allow a very low and uniform background to be reached. Very briefly, we show here what kind of background rejection can be applied:

- **Amplitude**. The spectroscopic capability of the GPD allows for setting a lower and an upper energy threshold.
- **Maximum window**. The ASIC CMOS chip can be configured setting a maximum allowed window frame. Background events are characterized by a window frame larger than that of an X-ray event.
- **Number of pixels**. X-rays provide a smaller non-zero pixel number with respect to the minimum ionizing background electrons.
- **Contiguity of the track**. Minimum ionizing particles produce tracks that can be discontinuous while this case is much more infrequent for higher ionizing particles such as X-ray photoelectrons.
- **Difference in skewness**. Background tracks due to minimum ionizing particle are characterized by a more uniform charge distribution with respect to photoelectron tracks, with a consequent difference in skewness.

Due to the finite range of the electrons, the most external pixel frame of the ASIC CMOS chip cannot be easily used because not all the azimuthal angles are detected with the same coverage. Such a frame represents a sort of side-anticoincidence that allows for excluding the background events arriving from the four sides. With the current GPD (see Fig. 9b) having a larger body with respect to that proposed for POLARIX, the background does not accumulate close to the ASIC edges.

Applying the above prescriptions, we expect that the background rate in orbit is conservatively well-estimated by means of past experiments with gas detectors filled with similar mixtures. We therefore evaluated the background of the GPD by using the measurements reported in [13] for the gas detector filled with Ne-CO_2 and extrapolating the results from the CH_4 gas detector but taking into account the difference in number of electrons in the molecules. The background estimates are shown in Table 2.

Table 2 Expected residual background for XIPE EXP

Source	Extension	Source rate(c/s)	Diff. Backg. (c/s)	Resid. Ne-CO_2 [13] (c/s)	Resid. CH_4 [13] (c/s)
Point-like	24" HEW (407 μm)	2 10^{-3}-200	5 10^{-12}	5.5 10^{-7} (4.8 nCrab)	5.6 10^{-6} (49 nCrab)
SgrB2	1.5' × 3.5' 1.5 × 3.5 mm^2	5.8 10^{-4} (5 μ Crab)	1.5 10^{-10}	1.8 10^{-5} (160 nCrab)	1.9 10^{-4} (1.6 μCrab)

5.2 The solar X-ray polarimeter and photometer

Polarimetry of solar flares is still a debated unresolved issue in astrophysics notwithstanding experiments launched since the beginning of X-ray astronomy. We decided to include in the payload two Medium Energy Solar Flare polarimeters (MESPs) designed with the same technology as the low energy polarimeters but filled with an Ar-DME (60–40) mixture. The drift region is 3-cm thick. The two MESPs always face the sun within an accepted angle of ±30° depending on the pointing constraints of the EXPs. Their open configuration is equipped with a field-of-view angular delimiter (FAD) that reduces the X-ray background, while the insertion of a multi-layer gray filter suppresses the low-energy, low-polarization, large photon flux expected during flares. The acquired data are continuously stored in a cyclic memory and, after a positive on-board trigger condition is verified, they are saved to be downloaded on-ground. The two MESPs are effective in the 15–35 keV energy range. At these energies, the intensity of the flare is still large, and a small geometrical area provides sufficient sensitivity. Also, the non-thermal bremsstrahlung starts to dominate the emission with an expected high degree of linear polarization.

Notwithstanding the intrinsic good imaging capability of MESP, no information on the location of the flare with respect to the solar limb can be directly derived by this open-sky configuration. The modelling of the expected polarization degree will, therefore, need information from other solar missions. The MESP design has already been developed for the New Hard X-ray Mission (NHXM, [123]) project and is validated in laboratory with a prototype 2-cm 2-atm thick filled with a mixture Ar-DME 70–30 [29]. To complement the study of the flare, an X-ray photometer, SphinX, uses a silicon PIN detector for high time resolution (10 μs) measurements of the solar spectra of quiet and active corona in the range 1.2–15 keV. The SphinX instrument is a heritage of CORONAS-Photon payload and its volume is 27 × 7 × 22 cm^3. A new more compact and lighter design is under study to be included in future missions [122].

Inclined penetration effects for the solar polarimeter The requirement on the sky visibility for EXP means that the pointing direction of MESP with respect to the Sun is ±30°. Photons coming from flares could therefore impinge on the

detector at an inclined angle. This effect has been studied for a GPD with a He-DME mixture in [78] and is the object of a forthcoming paper [77]. In [78], it has been shown that when applying the standard analysis to the modulation curve, prominent systematic effects are observed which can, however, be precisely corrected with the procedure described in the same paper. Moreover, recent laboratory measurements by the Space Research Center in Poland also showed that, with this inclination, SphinX is still sensitive for observing the emission from the Sun.

5.3 The electronics and the filter wheel

In the vicinity of each of the two GPDs of the EXP and of both of the two GPD of the MESP the three Back-End Electronics (BEE) are located. Each BEE is responsible for distributing the low voltages to the ASIC CMOS, controlling, by means of a dedicated Field-Programmable Gate Array (FPGA), the ASIC CMOS, performing Analog-to-Digital (A/D) conversion of the ASIC output signals, as well as the zero-suppression, time-tagging each event with an accuracy of 2 μs, and, finally, implementing a Peltier Driver 'for the GPD temperature control to be compliant with the GPD stability requirement (± 2 °C within $+5$ °C/ $+$ 20 °C). Each GPD requires three high voltage power supply lines (HV) in the range 0.2–3 kV (EXP) and 0.2–6 kV (MESP) and currents of a few nanoamperes.

Two filter wheels (FW #1 and FW #2), whose design is derived from that successfully flying on board XMM-Newton, are placed in front of each of the two EXP GPDs. Each observation mode corresponds to a different FW position. Each position allows for optimizing polarimetry in case of bright or multiple sources in the FoV, for calibrating the gain and the response to polarized X-rays [79] and for the gathering of the internal background. The GPD, the BEE and the FW compose the separated Focal Plane Assembly (FPA) of each EXP MM.

5.4 The interface electronics

XIPE takes advantage of the spacecraft On Board Data Handling unit (OBDH) in order to share with the bus some of the most relevant functionality such as the data-storing and the preparation of packets, at variance with POLARIX with its dedicated Payload Data Handling Unit (PDHU).

At the payload level, there is an Interface Electronics (I/FE) with the remaining functionalities. The I/FE is responsible for configuring the BEEs of EXP, MESP and SphinX, including the provision of regulated Low Voltages (LV) from the unregulated power provided by the solar panels. generating and managing the housekeeping, being in charge of the EXP FWs, taking care of the non regulated primary power bus providing the secondary voltages needed by the units, managing the Pulse Per Second synchronization signal line, parsing and executing the telecommands coming from the spacecraft, and managing the Payload Instrument Operative Modes (Boot, Maintenance, Idle, Observation and Test).

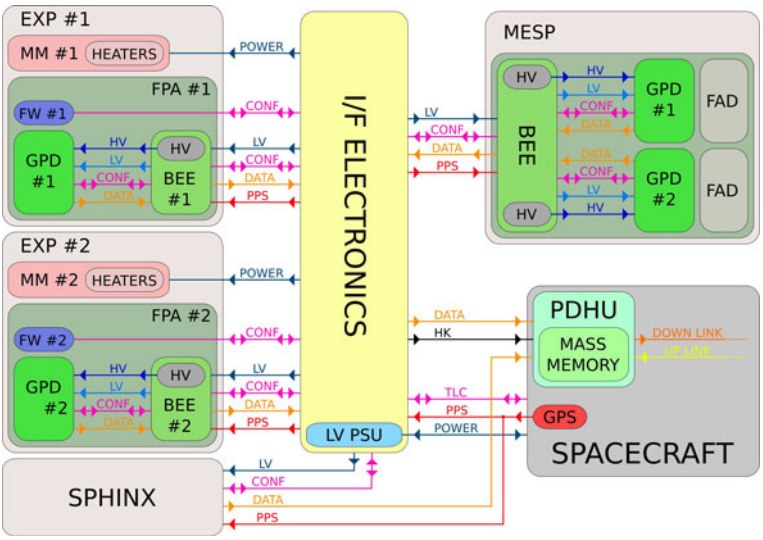

Fig. 10 The Block Diagram of the XIPE experiment. Here FW is the Filter Wheel (one for each of the two EXPs) that includes filters, unpolarized and polarized calibration sources; LV is the regulated low voltage that powers the three Back End Electronics (BEE) that include also the high voltages (HV), and manage the GPDs; MM is the X-ray Mirror Module (two MMs in total), FAD (field angular delimiter) is the mechanical shield for the Cosmic X-ray Background to be used in front of the solar X-ray flares polarimeter; PDHU is the payload data handling unit hosted in the spacecraft and incorporating the XIPE mass memory

6 Some results from the GPD-JETX mirror calibration at the PANTER X-ray test facility

The block diagram of the XIPE payload is shown in Fig. 10, here we show the first calibration of an X-ray polarimeter with X-ray optics, namely one of the two flight models of JET-X, has been performed at the Max Planck Institute for Extraterrestrial Physics PANTER X-ray test facility at Neuried by Munchen (Germany), see Fig. 11.

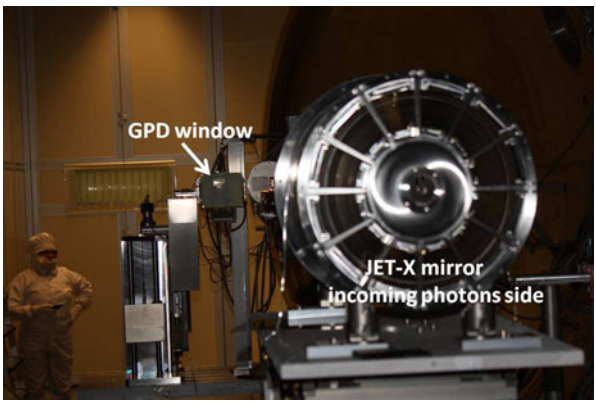

Fig. 11 The JET-X mirror in the front and the GPD in the background in the experimental chamber at the PANTER X-ray test facility

Table 3 On-axis theoretical and measured effective area during the November 2012 calibration campaign at the PANTER X-ray test facility

Energy (keV)	Measured effective area (cm^2)	Theoretical effective area (cm^2)
2.99	109	105
4.54	112	110
6.4	96	104
8.04	53	61

A stand-alone new calibration of the JET-X optics was performed with very good results, implying that JET-X optics are still suitable for an X-ray space experiment. Here, we present the preliminary re-measurement of the effective area (see Table 3) compared with theoretical expectations.

By means of Monte Carlo simulations and measurements, we already showed that the overall angular resolution is dominated by the point spread function of the optics and, secondarily, by the inclined penetration in the gas drift thickness [61, 114]. In this regard, we measured [28] at the PANTER X-ray test facility a position resolution, at 4.5 keV, of 23.2 arcsec, fully consistent with the estimate done at this energy. In Fig. 12 we show the image of the X-ray source at 4.5 keV focused by the optics and detected by the GPD.

We also performed a dedicated long run to arrive at a useful upper limit on the spurious modulation introduced by the optics at 4.5 keV. The results of this analysis, that require a careful evaluation of the modulation from the underlying bremsstrahlung, will be presented in a forthcoming paper. We plan in the future to perform an end-to-end calibration with the use of a polarized source at the same facility.

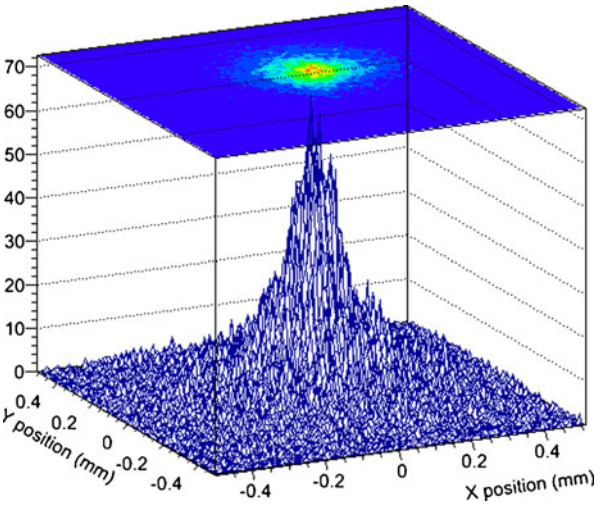

Fig. 12 Image of the PANTER X-ray source at 4.5 keV, focused by the JET-X optics and imaged by the GPD. The Z axis represents the total counts per bin. The focal length of the JET-X optics for a point source at infinite is 3500 mm while the focal length for the finite distance at PANTER X-ray facility is 3600 mm. The Half Energy Width measured at PANTER in this configuration corresponds to 23.2 arcsec while the plate scale is about 1 arcmin/mm

7 The payload budgets

The XIPE telemetry budget is reported in Table 4. The typical data rate for the two EXP units observing a typical source (with a flux of 200 mCrab) is 29 kbit/s, plus the housekeeping (4 kbit/s in total). For the purpose of sustaining high data rates in the case of bright sources, two strategies can be envisaged in the proposed architecture. The baseline is the temporary data storage in the PDHU mass memory, which is part of the spacecraft, combined with alternating between bright and faint sources in the observation sequence so that the average data rate is below that sustainable by the downlink. In this scenario, the PDHU mass memory dedicated to the two EXP units must be $> 2\ GB$ to store the data collected in a observation lasting 10^5 s of a bright source such as the Crab Nebula. Alternatively, the PDHU can perform in real-time the track reconstruction, and transmit on ground only the main results of the analysis. MESP data will be continuously transferred and stored in the PDHU but they will be transmitted to Earth only if a flare is detected. This is expected to occur sporadically: about 20 solar flare events lasting a few tens of minutes will be observed by the MESP during the mission lifetime of 2 years. In case of a trigger, the data starting from 5 min before the trigger will be completely downloaded, that is, without real-time on-board analysis, together with EXP data. The PDHU mass memory dedicated to MESP must be at least 2.5 GB to completely store the data collected for a X10 class flare (the brightest kind of event) lasting 30 min. The telemetry requirement for the SphinX instrument is 8 kbit/s.

The XIPE payload mass budget is reported in Table 5. XIPE is directly derived from POLARIX phase A and also benefits from a study for IXO, a proposed ESA large mission. The payload mass budget is therefore well-known. The mass of the flight telescopes, which contribute a large part of the mass, is known because they already exist. The GPD prototypes currently in use are already built with flight components; therefore, their (low) mass can be evaluated with high accuracy. The associated electronics for the XIPE detector payload has a standard design. Therefore, a definite evaluation of the mas of the flight hardware is possible. The payload structure is the large mounting plate, indeed part of the payload, where the mirrors, the detectors and their electronics are fixed.

Finally, the XIPE power budget is shown in Table 6. A large fraction of the power is for the thermal balancing of the Mirror Modules in order to prevent possible distortion due to temperature gradients. Taking into account that one JET-X telescope is currently flying on the Swift satellite, that the lower energy threshold is larger (2 keV for XIPE) and finally that the overall angular resolution is also determined by the inclined penetration in the GPD, the requested power for the telescope thermal stability is known, and is less demanding than that of XRT-SWIFT.

Table 4 XIPE Telemetry budget

2 × EXP units	29 kbit/s (typical)
MESP	< 2.5 GB (sporadically, once per month)
SphinX	8 kbit/s
HK	< 4 kbit/s

Table 5 The Payload Mass budget of XIPE. CBE is the Current Best Estimate and DMM is the Design Maturity Margin (it includes an additional cautionary percentage depending on the maturity level of each items, FAD is the Field Angular Delimiter for the solar polarimeter (MESP)

	Payload mass budget					
	No. of item	CBE		DMM	CBE+DMM	
		Mass (kg)	Tot (kg)		Mass (kg)	Mass (kg)
EXP						203.6
MM	2	60a	120.0	5 %	126.0	
MM baffles + heater + harness	2	5.0a	10.0	5 %	10.5	
MM mounting structure	1	10.0	10.0	20 %	12.0	
GPD+FW+Baffle+mech. interf.	2	3.3b	6.6	10 %	7.3	
BEE+mech interf.	2	1.6b	3.1	10 %	3.4	
Payload structure	1	32.0	32.0	20 %	38.4	
Sun Shield	1	5.0	5.0	20 %	6.0	
MESP						16.0
GPD+mech interf.	2	3.0	6.0	10 %	6.6	
BEE+mech interf.	1	2.0	2.0	10 %	2.2	
FAD	2	3.0	6.0	20 %	7.2	
SPHINX						3.7
All integrated instrument	1	3.5	3.5	5 %	3.7	
Other						10.7
StarTracker	1	1.0	1.0	5 %	1.1	
I/FE	1	5.0	5.0	20 %	6.0	
Harness	1	3.0	3.0	20 %	3.6	
						Total
						234.0

[a]POLARIX heritage

[b]IXO heritage

8 Mission profile

8.1 Proposed launch vehicle

The mission concept is based on a launch into a circular, low equatorial orbit by the Vega Launcher. The orbit considered for XIPE is of Low Earth Orbit (LEO) type, and has characteristics is reported in Table 8.

8.2 Mission duration

The nominal mission duration is 2 years, plus 1 month for commissioning, 3 months for the Science Verification Phase (SVP) and 1 month for decommissioning. Such a duration is sufficient to address the science goal presented in Section 2.

Table 6 The payload power budget of XIPE

	Payload power budget					
	No. of item	CBE		DMM	CBE+DMM	
		Power(W)	Power (W)		Power (W)	Power (W)
EXP						168.0
MM thermal control (peak)	2	50a	100.0	20 %	120.0	
GPD	2	2.0b	4.0	20 %	4.8	
BEE	2	12.0b	24.0	20 %	28.8	
FW (peak)	2	6.0b	12.0	20 %	14.4	
MESP						28.8
GPD	2	2.0	4.0	20 %	4.8	
BEE	1	20.0	20.0	20 %	24.0	
SPHINX						15.8
All integrated instrument (peak)	1	15	15.0	5 %	15.8	
Other						29.5
StarTracker	1	6.0	6.0	5 %	6.3	
I/FE	1	19.3	19.3	20 %	23.2	
						Total
						242.1

[a]Swift heritage

[b]IXO heritage

8.3 Ground station

The satellite in nominal operation phase is supported by a dedicated low latitude ground station, such as Malindi, during its entire lifetime. The Malindi ground station is optimally located for the near equatorial XIPE-satellite orbit. The coverage pattern for this LEO altitude is a regular sequence of contacts, 15 per day, once per orbit, each one followed by a gap of about 85 min. Assuming this contact time and a telemetry data rate as high as 512 kbps (included Reed-Solomon on-board coding for error correction managing), the downloadable data volume is 3.25 Gb/day.

Table 7 System constraints of XIPE

Constrain	Value
Satellite stabilization	Three axis
Absolute pointing error	3 arcmin
Absolute measurement accuracy	10 arcsec, 5 Hz
Sky accessibility	$90° \pm 30°$
Average scientific telemetry rate	50 kbit/s
Minimum size storage	5 GByte

Table 8 Requirements on the launcher

Parameter	Requirement
Altitude	600 ±16 km for 2 years mission and controlled re-entry.
Inclination	5° ± 1°
Eclipse duration	36 minutes max
Ground Station	8–11 min contact

8.4 Communication requirements

The communication requires, as a minimum, the use of S-Band communication system, which is available at Malindi Ground Station. This is made compatible with the mission goals by means of alternating the observation of bright source with subsequent observation of dim sources, coupled with storage of the data in the on-board memory.

8.5 Ground segment

The XIPE Ground Segment (G/S) performs the main functions/operations needed at ground level to manage the mission in terms of both satellite control and global data management. The planned G/S includes the ground station of the Italian Space Agency (ASI) located at Malindi and the Mission Operation Center (MOC) of INPE at São José dos Campos (Brazil). The G/S monitors and controls the satellite platform and payload, performs the orbit/attitude operations and generates the orbital products used for satellite Monitoring & Control, for the payload management and mission planning. The G/S generates the mission planning and checks, according to scientific observation requests coming from the User Segment (U/S). It acquires the raw satellite data (housekeeping and telemetry) and it transfers them to the U/S for processing. The G/S also includes the Satellite Simulator and the Communication Network responsible for interconnecting the Ground Segment facilities and providing the related communication services in a secure and reliable way.

The U/S manages the scientific observation requests coming from the scientific community, forwards them to the G/S for payload scheduling activities, ingests the raw satellite data coming from the G/S, and generates, archives, catalogues and delivers the scientific data and the data products to the user community.

8.6 Alternative mission scenario

The utilization of Iridium Next, at variance with the bus proposed for POLARIX, also gives the opportunity for significative launch cost reduction by means of participation in twin or a dedicated launch with DNEPR (also called SS18), an ukraine launch vehicle named after the Dnieper River, with a more favorable cost with respect to Vega. This alternative has not been studied so far. It would imply a highly inclined

orbit. The expected background would be larger in this case, but we should not forget that its counting rate is smaller than the source counting rate by orders of magnitude for any observation with realistic observing time for X-ray polarimetry.

9 System requirements and spacecraft key factors

The key constraints on the satellite characteristics are shown in Table 7. The photoelectric X-ray polarimeters are based on GPD technology, a non-dispersive instrument with intrinsic homogeneous azimuthal response irrespective of the conversion point of the photons in the gas. Therefore, rotation is not required since the systematics induced by grazing incidence X-ray optics are not expected to provide additional instrumental contribution unless down to a very low level [106]. This fact facilitates the use of platforms with the usual three-axis stabilization. The requirement on the Spacecraft Absolute Pointing Error is driven by the FoV of the instrument and by the requirement on the misalignment of the two optics. The requirement on the Absolute Measurement Accuracy allows for not degrading the PSF of the instruments and it exploits the capability of the GPD to measure the conversion point with high precision and the photon-by-photon transmission on-ground. The XIPE science data down-link and storage capability are compatible with S-band to observe an average source. A storage of 5 GByte allows the acquisition of 24 h of data from Crab plus an X-ray flare of class X10.

Some operations, usually performed at payload level, are in this case demanded of the hardware installed at bus (platform) level. This is possible because of the characteristics of the proposed platform. The OBDH acquires and stores the science data, taking care of the satellite telecommands, of the telemetry and of the attitude control (AOCS). The thermal control, including that of the telescopes and of the detectors, is also performed by the OBDH.

The on-board processor, with associated electronics and memory, decodes and distributes the payload telecommand. It processes, if needed, the data evaluating the impact point and the photoelectron emission angle, and packets the data and the Housekeeping, storing them in the OBDH memory. Finally, it manages the Pulse Per Second synchronization signal (for the On-Board Timing(OBT) and Universal Time (UT) synchronization) line by using the GPS system. The accuracy and precision of the on-board clock should be such to time tag the event with 2 μs accuracy.

10 The platform for XIPE

The size and pointing requirements for the XIPE telescopes are the drivers for the selection of the XIPE service module. In this framework, the utilization of the Iridium Next platform, developed by Thales Alenia Space firm on behalf of Iridium Communication Inc., is very promising. This product is now commercialized with the name of Elite platform. The advantages of this three-axis stabilized platform is in the cost resulting from the mass production of 81 satellites. Also, the mass production fits perfectly the launch date in 2017. The utilization of this kind of platform for an

X-ray mission is not a novelty because it has been already considered for other science missions.

The Iridium Next platform is equipped with a 2.0 kW solar array mounted on a double articulated arm. The high modularity of the platform allows for the "plug & play" of the payload module. By means of a preliminary payload accommodation study, a XIPE satellite concept based on Elite platform was developed in collaboration with Thales Alenia Space Italia. This concept is shown in Fig. 13.

Iridium Next can also provide an option based on X-band down-link transmission and a propulsion capability, allowing the orbit maintenance (if necessary) as well as the management of satellite end-of-life. The Iridium Next platform and the Vega launcher can be matched by means of a special adapter. The accommodation of XIPE within the fairing of the VEGA launcher is shown in Fig. 14.

The platform and the payload can also be concurrently integrated and tested at a very late stage, reducing interference and therefore optimizing the schedule. The Iridium platform mass is about 450 kg and the power consumption is about 500 W.

11 Science operation and archiving

The XIPE science operation and archiving are different from those of standard ESA missions. The team owns the Science Operation Phase data, lasting 3 months, and the Core program data for 25 % of the net observing time. The remaining 75 % net observing time is assigned to a peer-reviewed Guest Observer program. Target of Opportunity observations are possible and a proprietary period of 1 year is guaranteed.

The data are, after a proper check and standard processing, delivered to the owner. They are in the form of a photon list containing the time, the absorption point, the

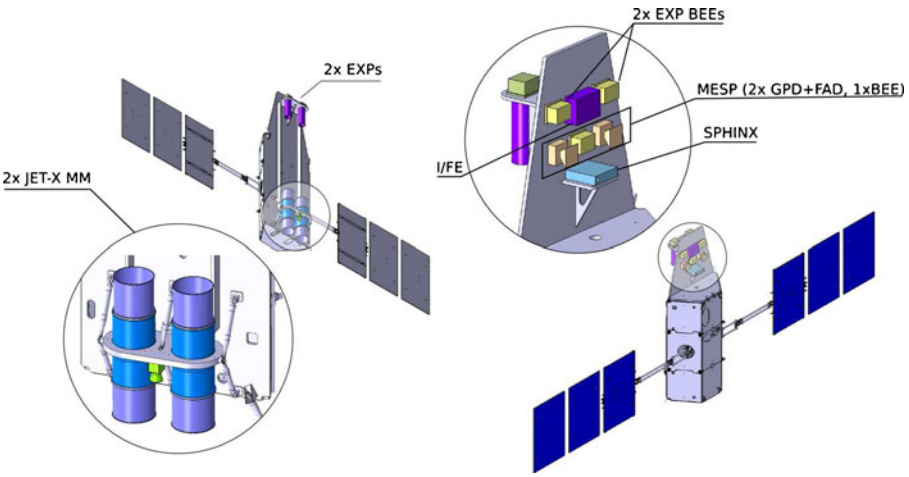

Fig. 13 XIPE payload accommodated in the Iridium NEXT bus

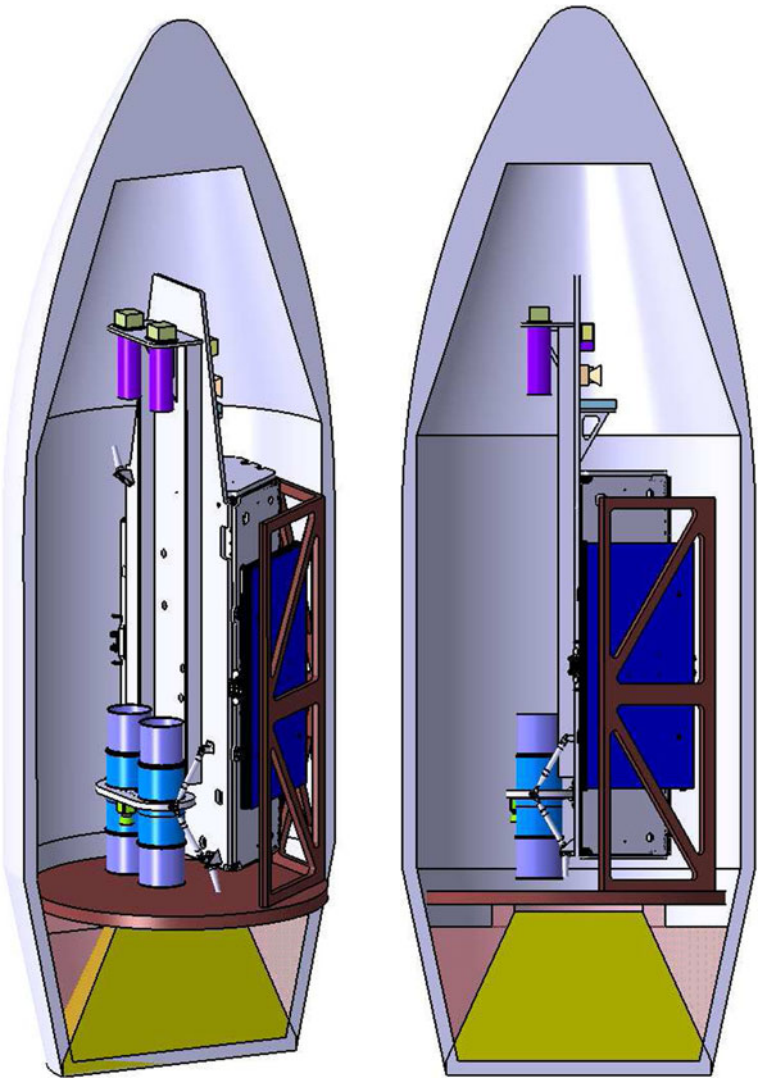

Fig. 14 XIPE satellite in the fairing of the VEGA bus

energy and the emission angle, plus the data on coverage, time windows and dead time. Specific nonstandard analysis is possible by means of a software package distributed and documented by the team of the Scientific Data Center of the Italian Space Agency (ASDC), that also stores all the data and products at their different steps. Data format and the calibration database (CALDB) are written in OGIP (Office of Guest Investigator Programs)-FITS (Flexible Image Transport System), that is the standard file format in X-ray astronomy, with a total expected amount of 5 terabyte. The Science Operation Center is located at the INAF/IAPS, INAF/OAB, INFN/Pisa and ASDC-Frascati.

12 Conclusions

The most recently flown dedicated X-ray polarimeter dates back to the 1970s. Motivated by the interest among theoreticians for opening a new window in X-ray astronomy, where almost all the classes of sources are expected to be polarized, many missions with on-board X-ray polarimetry have been proposed since then, and some arrived at various levels of completion. These include the fully tested and calibrated *Stellar X-ray Polarimeter* [52, 53, 112, 128] aboard the former and not flown Spectrum X-Gamma Russian satellite, and GEMS, that was discontinued by NASA in May 2012.

In this paper, we described XIPE, proposed in June 2012 for an ESA small mission aimed at performing spectral-imaging polarimetry of celestial sources and of solar flares. XIPE takes advantage of already existing X-ray optics with good imaging capabilities and an already existing improved version of the GPD X-ray polarimeter, built with materials and techniques already suitable for use in space. XIPE is a low-risk mission with a limited need for resources. The MDP that XIPE can reach (14 % at 1 mCrab in 10^5 s of observing time in 2–10 keV energy band) is compliant with the polarization expected by most of the classes of galactic sources and with a limited sample of luminous AGNs.

The imaging capability allows for resolving polarimetry of the Crab and of other PWN and supernova remnants, disentangling the presence of multiple sources in the FoV and maintaining the background at a level compatible with making all observations source dominated. The feasibility of XIPE has been further demonstrated by having tested the proposed JET-X optics, either stand-alone or with the GPD gas detector in its focus, in a dedicated calibration campaign at the PANTER X-ray test facility.

Acknowledgments This work is partially funded by ASI, INAF and INFN.

References

1. Amelino-Camelia, G.: Phenomenology of Planck-scale Lorentz-symmetry test theories. New J. Phys. **6**, 188 (2004). doi:10.1088/1367-2630/6/1/188. arXiv:gr-qc/0212002
2. Angel, J.R., Novick, R., vanden Bout, P., Wolff, R.: Search for X-ray Polarization in Sco X-1. Phys. Rev. Lett. **22**, 861–865 (1969). doi:10.1103/PhysRevLett.22.861
3. Araya, M., Cui, W.: Evidence for cosmic ray acceleration in Cassiopeia A. ApJ **720**, 20–25 (2010). doi:10.1088/0004-637X/720/1/20. arXiv:1006.5962
4. Bai, T., Ramaty, R.: Backscatter, anisotropy, and polarization of solar hard X-rays. ApJ **219**, 705–726 (1978). doi:10.1086/155830
5. Bassan, N., Mirizzi, A., Roncadelli, M.: Axion-like particle effects on the polarization of cosmic high-energy gamma sources. JCAP **5**, 010 (2010). doi:10.1088/1475-7516/2010/05/010. arXiv:1001.5267
6. Bellazzini, R., et al: A polarimeter for IXO. In: Bellazzini, R., Costa, E., Matt, G., Tagliaferri, G. (eds.) X-ray Polarimetry: A New Window in Astrophysics by Ronaldo Bellazzini, Enrico Costa, Giorgio Matt and Gianpiero Tagliaferri, p. 269. Cambridge University Press, Cambridge (2010). ISBN: 9780521191845

7. Bellazzini, R., Angelini, F., Baldini, L., Brez, A., Costa, E., Di Persio, G., Latronico, L., Massai, M.M., Omodei, N., Pacciani, L., Soffitta, P., Spandre, G.: Novel gaseus X-ray polarimeter: data analysis and simulation. In: Proceedings SPIE, vol. 4843, p. 383 (2003)
8. Bellazzini, R., Spandre, G., Minuti, M., Baldini, L., Brez, A., Cavalca, F., Latronico, L., Omodei, N., Massai, M.M., Sgro', C., Costa, E., Soffitta, P., Krummenacher, F., de Oliveira, R.: Direct reading of charge multipliers with a self-triggering CMOS analog chip with 105 k pixels at 50 μm pitch. Nucl. Inst. Methods Phys. Res. A **566**, 552 (2006). doi:10.1016/j.nima.2006.07.036. arXiv:physics/0604114
9. Bellazzini, R., Spandre, G., Minuti, M., Baldini, L., Brez, A., Latronico, L., Omodei, N., Razzano, M., Massai, M.M., Pesce-Rollins, M., Sgró, C., Costa, E., Soffitta, P., Sipila, H., Lempinen, E.: A sealed Gas Pixel Detector for X-ray astronomy. Nucl. Inst. Methods Phys. Res. A **579**, 853 (2007). doi:10.1016/j.nima.2007.05.304. arXiv:astro-ph/0611512
10. Bellazzini, R., Brez, A., Costa, E., Minuti, M., Muleri, F., Pinchera, M., Rubini, A., Soffitta, P., Spandre, G.: Photoelectric X-ray polarimetry with gas pixel detectors. Nucl. Inst. Methods Phys. Res. A. **730**, 173 (2013)
11. Bleeker, J.A.M., Willingale, R., van der Heyden, K., Dennerl, K., Kaastra, J.S., Aschenbach, B., Vink, J.: Cassiopeia A: On the origin of the hard X-ray continuum and the implication of the observed O Viii Ly-alpha /Ly-beta distribution. A&A **365**, L225–L230 (2001). doi:10.1051/0004-6361:20000048. arXiv:astro-ph/0010606
12. Brown, J.C.: The deduction of energy spectra of non-thermal electrons in flares from the observed dynamic spectra of hard X-ray bursts. Sol. Phys. **18**, 489–502 (1971). doi:10.1007/BF00149070
13. Bunner, A.N.: Soft X-ray results from the Wisconsin experiment on OSO-8. ApJ **220**, 261–271 (1978)
14. Burrows, D.N., Hill, J.E., Nousek, J.A., Kennea, J.A., Wells, A., Osborne, J.P., Abbey, A.F., Beardmore, A., Mukerjee, K., Short, A.D.T., Chincarini, G., Campana, S., Citterio, O., Moretti, A., Pagani, C., Tagliaferri, G., Giommi, P., Capalbi, M., Tamburelli, F., Angelini, L., Cusumano, G., Bräuninger, H.W., Burkert, W., Hartner, G.D.: The swift X-ray telescope. Space Sci. Rev. **120**, 165–195 (2005). doi:10.1007/s11214-005-5097-2. arXiv:astro-ph/0508071
15. Celotti, A., Matt, G.: Polarization properties of synchrotron self-compton emission. MNRAS **268**, 451–458 (1994)
16. Churazov, E., Sunyaev, R., Sazonov, S.: Polarization of X-ray emission from the Sgr B2 cloud. MNRAS **330**, 817–820 (2002). doi:10.1046/j.1365-8711.2002.05113.x. arXiv:astro-ph/0111065
17. Citterio, O., Campano, S., Conconi, P., Ghigo, M., Mazzoleni, F., Poretti, E., Conti, G., Cusumano, G., Sacco, B., Brauninger, H., Burkert, W., Egger, R., Castelli, C.M., Willingale, R.: Characteristics of the flight model optics for the JET-X telescope onboard the Spectrum-X-Gamma satellite. In: Hoover, R.B., Walker, A.B. (eds.) Society of Photo-Optical Instrumentation Engineers (SPIE) Conference Series, Society of Photo-Optical Instrumentation Engineers (SPIE) Conference Series, vol 2805, pp 56–65 (1996)
18. Connors, P.A., Stark, R.F., Piran, T.: Polarization features of X-ray radiation emitted near black holes. ApJ **235**, 224 (1980). doi:10.1086/157627
19. Costa, E., Soffitta, P., Bellazzini, R., Brez, A., Lumb, N., Spandre, G.: An efficient photoelectric X-ray polarimeter for the study of black holes and neutron stars. Nature **411**, 662 (2001). arXiv:astro-ph/0107486
20. Costa, E., Bellazzini, R., Tagliaferri, G., Matt, G., Argan, A., Attinà, P., Baldini, L., Basso, S., Brez, A., Citterio, O., di Cosimo, S., Cotroneo, V., Fabiani, S., Feroci, M., Ferri, A., Latronico, L., Lazzarotto, F., Minuti, M., Morelli, E., Muleri, F., Nicolini, L., Pareschi, G., di Persio, G., Pinchera, M., Razzano, M., Reboa, L., Rubini, A., Salonico, A.M., Sgro', C., Soffitta, P., Spandre, G., Spiga, D., Trois, A.: POLARIX: A pathfinder mission of X-ray polarimetry. Exp. Astron. **28**, 137–183 (2010). doi:10.1007/s10686-010-9194-1. arXiv:1105.0637
21. Dean, A.J., Clark, D.J., Stephen, J.B., McBride, V.A., Bassani, L., Bazzano, A., Bird, A.J., Hill, A.B., Shaw, S.E., Ubertini, P.: Polarized gamma-ray emission from the crab. Science **321**, 1183 (2008). doi:10.1126/science.1149056
22. Deutsch, A.J.: The electromagnetic field of an idealized star in rigid rotation in vacuo. Annales d'Astrophysique **18**, 1 (1955)
23. Doschek, G.A.: X-ray and EUV Observations of Solar Flares. In: Favata, F., Drake, J.J. (eds.) Stellar Coronae in the Chandra and XMM-NEWTON Era, Astronomical Society of the Pacific Conference Series, vol 277, p 89 (2002)

24. Dovčiak, M., Muleri, F., Goosmann, R.W., Karas, V., Matt, G.: Thermal disc emission from a rotating black hole: X-ray polarization signatures. MNRAS **391**, 32–38 (2008). doi:10.1111/j.1365-2966.2008.13872.x. arXiv:0809.0418
25. Dovčiak, M., Muleri, F., Goosmann, R.W., Karas, V., Matt, G.: Light-bending scenario for accreting black holes in X-ray polarimetry. ApJ **731**, 75 (2011). doi:10.1088/0004-637X/731/1/75. arXiv:1102.4247
26. Elsner, R.F., O'Dell, S.L., Weisskopf, M.C.: Measuring X-ray polarization in the presence of systematic effects: known background. In: Society of Photo-Optical Instrumentation Engineers (SPIE) Conference Series, Society of Photo-Optical Instrumentation Engineers (SPIE) Conference Series, vol. 8443 (2012). doi:10.1117/12.924889 arXiv:1208.0610
27. Emslie, A.G., Brown, J.C.: The polarization and directivity of solar-flare hard X-ray bremsstrahlung from a thermal source. ApJ **237**, 1015–1023 (1980). doi:10.1086/157947
28. Fabiani, S. et al.: The imaging properties of the Gas Pixel Detector as a focal plane polarimeter. submitted (2013)
29. Fabiani, S., Bellazzini, R., Berrilli, F., Brez, A., Costa, E., Minuti, M., Muleri, F., Pinchera, M., Rubini, A., Soffitta, P., Spandre, G.: Performance of an Ar-DME imaging photoelectric polarimeter. In: Society of Photo-Optical Instrumentation Engineers (SPIE) Conference Series, Society of Photo-Optical Instrumentation Engineers (SPIE) Conference Series, vol. 8443 (2012). doi:10.1117/12.925374
30. Fan, Y.Z., Wei, D.M., Xu, D.: γ-ray burst ultraviolet/optical afterglow polarimetry as a probe of quantum gravity. MNRAS **376**, 1857–1860 (2007). doi:10.1111/j.1365-2966.2007.11576.x. arXiv:astro-ph/0702006
31. Fernández, R., Davis, S.W.: The X-ray polarization signature of quiescent magnetars: effect of magnetospheric scattering and vacuum polarization. ApJ **730**, 131 (2011). doi:10.1088/0004-637X/730/2/131. arXiv:1101.0834
32. Gambini, R., Pullin, J.: Nonstandard optics from quantum space-time. Phys. Rev. D **59**(12), 124,021 (1999). arXiv:gr-qc/9809038
33. Gleiser, R.J., Kozameh, C.N.: Astrophysical limits on quantum gravity motivated birefringence. Phys. Rev. D **64**(8), 083007-1 (2001). doi:10.1103/PhysRevD.64.083007. arXiv:gr-qc/0102093
34. Goosmann, R.W., Matt, G.: Spotting the misaligned outflows in NGC 1068 using X-ray polarimetry. MNRAS **415**, 3119–3128 (2011). doi:10.1111/j.1365-2966.2011.18923.x. arXiv:1012.4652
35. Gotthelf, E.V., Koralesky, B., Rudnick, L., Jones, T.W., Hwang, U., Petre, R.: Chandra detection of the forward and reverse shocks in Cassiopeia A. ApJ **552**, L39–L43 (2001). doi:10.1086/320250. arXiv:astro-ph/0104161
36. Gowen, R.A., Cooke, B.A., Griffiths, R.E., Ricketts, M.J.: An upper limit to the linear X-ray polarization of SCO X-1. MNRAS **179**, 303–310 (1977)
37. Grandi, P., Palumbo, G.G.C.: Jet and accretion-disk emission untangled in 3C 273. Science **306**, 998–1002 (2004). doi:10.1126/science.1101787
38. Grandi, P., Palumbo, G.G.C.: Broad-line radio galaxies: jet contribution to the nuclear X-ray continuum. ApJ **659**, 235–240 (2007). doi:10.1086/510769
39. Gunji, S., et al.: Performance of hard X-ray polarimeter: PHENEX. In: Bellazzini, R., Costa, E., Matt, G., Tagliaferri, G. (eds.) X-ray Polarimetry: A New Window in Astrophysics by Ronaldo Bellazzini, Enrico Costa, Giorgio Matt and Gianpiero Tagliaferri. Cambridge University Press. ISBN: 9780521191845, p. 350, (2010)
40. Haardt, F., Matt, G.: X-ray polarization in the two-phase model for AGN and X-ray binaries. MNRAS **261**, 346–352 (1993)
41. Harding, A.K.: Emission from rotation-powered pulsars: is it all relative? In: Chen, P., Bloom, E., Madejski, G., Patrosian, V. (eds.) 22nd Texas Symposium on Relativistic Astrophysics, pp 149–158 (2005). arXiv:astro-ph/0503300
42. Heisemberg, W., Euler, H.: Consequences of Dirac's theory of positrons. Z. Phys. **98**, 714 (1936)
43. Heyl, J.S., Shaviv, N.J.: Polarization evolution in strong magnetic fields. MNRAS **311**, 555–564 (2000). doi:10.1046/j.1365-8711.2000.03076.x. arXiv:astro-ph/9909339
44. Heyl, J.S., Shaviv, N.J., Lloyd, D.: The high-energy polarization-limiting radius of neutron star magnetospheres—I. Slowly rotating neutron stars. MNRAS **342**, 134–144 (2003). doi:10.1046/j.1365-8711.2003.06521.x. arXiv:astro-ph/0302118
45. Hill, J.E., Baker, R.G., Black, J.K., Browne, M.J., Baumgartner, W.H., Caldwell, E.M., Cantwell, J.D., Davies, A., Desai, A.B., Dickens, P.L., Dobson, N.K., Foxwell, R.L., Francomacaro, A.S., Gall,

D., Gregory, K.J., Griffiths, S., Hayato, A., Hampshire, R.O., Hwang, T., Jhabvala, M.D., Jahoda, K., Kaaret, P., Lehtonen, S.J., Martin, N.F., Mohammed, J.S., Montt de Garcia, K., Morell, A., Nolan, D.S., Russell, R.E., Sampson, M.A., Sanders, J.A., Simms, K., Singer, M.J., Swank, J.H., Tamagawa, T., Weaver, A., Yerushalmi, S.N., Xu, J.J.: The design and qualification of the GEMS x-ray polarimeters. In: Society of Photo-Optical Instrumentation Engineers (SPIE) Conference Series, Society of Photo-Optical Instrumentation Engineers (SPIE) Conference Series, vol. 8443 (2012). doi:10.1117/12.928435

46. Horák, J., Karas, V.: On the role of strong gravity in polarization from scattering of light in relativistic flows. MNRAS **365**, 813–826 (2006). doi:10.1111/j.1365-2966.2005.09748.x. arXiv:astro-ph/0510532
47. Hughes, J.P., Long, K.S., Novick, R.: A search for X-ray polarization in cosmic X-ray sources. ApJ **280**, 255 (1984). doi:10.1086/161992
48. Iwahashi, T., Tamagawa, T., Hayato, A., Nakamura, S., Konami, S., Asami, F., Yasuda, N., Kitamura, H., Sakurai, H., Tokanai, F., Miyasaka, H., Makishima, K.: Heavy ion and proton irradiation of gas electron multipliers with liquid crystal polymer insulator: evaluation tests for use in space. IEEE Trans. Nucl. Sci. **58**, 2401–2406 (2011). doi:10.1109/TNS.2011.2162001
49. Jahoda, K.: The gravity and extreme magnetism small explorer. In: Society of Photo-Optical Instrumentation Engineers (SPIE) Conference Series, Society of Photo-Optical Instrumentation Engineers (SPIE) Conference Series, vol. 7732 (2010). doi:10.1117/12.857439
50. Jeffrey, N.L.S., Kontar, E.P.: Spatially resolved hard X-ray polarization in solar flares: effects of Compton scattering and bremsstrahlung. A&A **536**, A93 (2011). doi:10.1051/0004-6361/201117987. arXiv:1110.4993
51. Kaaret, P.: X-ray clues to viability of loop quantum gravity. Nature **427**, 287 (2004)
52. Kaaret, P., Novick, R., Martin, C., Hamilton, T., Sunyaev, R., Lapshov, I., Silver, E., Weisskopf, M., Elsner, R., Chanan, G., Manzo, G., Costa, E., Fraser, G., Perola, G.C.: SXRP. A focal plane stellar X-ray polarimeter for the SPECTRUM-X-Gamma mission. In: Hoover RB (ed) Society of Photo-Optical Instrumentation Engineers (SPIE) Conference Series, Society of Photo-Optical Instrumentation Engineers (SPIE) Conference Series, vol 1160, pp. 587–597 (1989)
53. Kaaret, P.E., Schwartz, J., Soffitta, P., Dwyer, J., Shaw, P.S., Hanany, S., Novick, R., Sunyaev, R., Lapshov, I.Y., Silver, E.H., Ziock, K.P., Weisskopf, M.C., Elsner, R.F., Ramsey, B.D., Costa, E., Rubini, A., Feroci, M., Piro, L., Manzo, G., Giarrusso, S., Santangelo, A.E., Scarsi, L., Perola, G.C., Massaro, E., Matt, G.: Status of the stellar x-ray polarimeter for the Spectrum-X-Gamma mission. In: Fineschi S (ed) Society of Photo-Optical Instrumentation Engineers (SPIE) Conference Series, Society of Photo-Optical Instrumentation Engineers (SPIE) Conference Series, vol. 2010, pp. 22–27 (1994)
54. Kalemci, E., Boggs, S.E., Kouveliotou, C., Finger, M., Baring, M.G.: Search for polarization from the prompt gamma-ray emission of GRB 041219a with SPI on INTEGRAL. ApJS **169**, 75–82 (2007). doi:10.1086/510676. arXiv:astro-ph/0610771
55. Kostelecký, V.A., Mewes, M.: Constraints on relativity violations from gamma-ray bursts. Phys. Rev. Lett. **110**(20), 201601 (2013). doi:10.1103/PhysRevLett.110.201601
56. Koyama, K., Maeda, Y., Sonobe, T., Takeshima, T., Tanaka, Y., Yamauchi, S.: ASCA View of our galactic center: Remains of past activities in X-Rays? PASJ **48**, 249–255 (1996)
57. Koyama, K., Inui, T., Matsumoto, H., Tsuru, T.G.: A time-variable X-Ray echo: indications of a past flare of the galactic-center black hole. PASJ **60**, 201–205 (2008). arXiv:0711.2853
58. Krawczynski, H.: Tests of general relativity in the strong-gravity regime based on X-Ray spectropolarimetric observations of black holes in X-Ray binaries. ApJ **754**, 133 (2012). doi:10.1088/0004-637X/754/2/133. arXiv:1205.7063
59. Lai, D., Ho, W.C.: Polarized X-ray emission from magnetized neutron stars: signature of strong-field vacuum polarization. Phys. Rev. Lett. **91**(7), 071,101 (2003). arXiv:astro-ph/0303596
60. Laurent, P., Götz, D., Binétruy, P., Covino, S., Fernandez-Soto, A.: Constraints on Lorentz invariance violation using integral/IBIS observations of GRB041219A. Phys. Rev. D **83**(12), 121301 (2011). doi:10.1103/PhysRevD.83.121301. arXiv:1106.1068
61. Lazzarotto, F., et al.: Angular resolution of a photoelectric polarimeter. In: Bellazzini, R., Costa, E., Matt, G., Tagliaferri, G. (eds.) X-ray Polarimetry: A New Window in Astrophysics by Ronaldo Bellazzini, Enrico Costa, Giorgio Matt and Gianpiero Tagliaferri. Cambridge University Press. ISBN: 9780521191845, p. 79 (2010)

62. Li, L., Narayan, R., McClintock, J.E.: Inferring the inclination of a black hole accretion disk from observations of its polarized continuum radiation. ApJ **691**, 847–865 (2009). doi:10.1088/0004-637X/691/1/847. arXiv:0809.0866
63. Maccione, L., Liberati, S., Celotti, A., Kirk, J.G., Ubertini, P.: γ-ray polarization constraints on Planck scale violations of special relativity. Phys. Rev. D **78**(10), 103003-1 (2008). doi:10.1103/PhysRevD.78.103003. arXiv:0809.0220
64. Marin, F., Goosmann, R., Dovčiak, M.: Modeling the optical/UV polarization while flying around the tilted outflows of NGC 1068. J. Phys. Conf. Ser. **372**(1), 012,065 (2012). doi:10.1088/1742-6596/372/1/012065. arXiv:1204.0936
65. Marin, F., Goosmann, R.W., Dovčiak, M., Muleri, F., Porquet, D., Grosso, N., Karas, V., Matt, G.: X-ray polarimetry as a new tool to discriminate reflection from absorption scenarios - predictions for MCG-6-30-15. MNRAS **426**, L101–L105 (2012). doi:10.1111/j.1745-3933.2012.01335.x. arXiv:1208.3314
66. Matt, G.: X-ray polarization properties of the accretion column in magnetic CVs. A&A **423**, 495–500 (2004). doi:10.1051/0004-6361:20035649. arXiv:astro-ph/0403238
67. Matt, G., Costa, E., Perola, G.C., Piro, L.: X ray polarization of the reprocessed emission from accretion disk in Seyfert galaxies. In: Hunt, J., Battrick, B. (eds.) Two Topics in X-Ray Astronomy, Volume 1: X Ray Binaries. Volume 2: AGN and the X Ray Background, ESA Special Publication, vol. 296, pp. 991–993 (1989)
68. McConnell, M.L., Bancroft, C., Bloser, P.F., Connor, T., Legere, J., Ryan, J.M.: GRAPE: a balloon-borne gamma-ray polarimeter. In: Society of Photo-Optical Instrumentation Engineers (SPIE) Conference Series, Society of Photo-Optical Instrumentation Engineers (SPIE) Conference Series, vol. 7435 (2009). doi:10.1117/12.826407
69. McGlynn, S., Clark, D.J., Dean, A.J., Hanlon, L., McBreen, S., Willis, D.R., McBreen, B., Bird, A.J., Foley, S.: Polarisation studies of the prompt gamma-ray emission from GRB 041219a using the spectrometer aboard INTEGRAL. A&A **466**, 895–904 (2007). doi:10.1051/0004-6361:20066179. arXiv:astro-ph/0702738
70. McNamara, A.L., Kuncic, Z., Wu, K.: X-ray polarization signatures of Compton scattering in magnetic cataclysmic variables. MNRAS **386**, 2167–2172 (2008). doi:10.1111/j.1365-2966.2008.13174.x. arXiv:0803.0350
71. Mèszàros, P.: High-energy Radiation from Magnetized Neutron Stars. Theoretical Astrophysics. University of Chicago Press, Chicago (1992)
72. Mèszàros, P., Novick, R., Szentgyorgyi, A., Chanan, G.A., Weisskopf, M.C.: Astrophysical implications and observational prospects of X-ray polarimetry. ApJ **324**, 1056 (1988). doi:10.1086/165962
73. Miller, L., Turner, T.J., Reeves, J.N.: The absorption-dominated model for the X-ray spectra of typeI active galaxies: MCG-6-30-15. MNRAS **399**, L69–L73 (2009). doi:10.1111/j.1745-3933.2009.00726.x. arXiv:0907.3114
74. Miniutti, G., Fabian, A.C.: A light bending model for the X-ray temporal and spectral properties of accreting black holes. MNRAS **349**, 1435–1448 (2004). doi:10.1111/j.1365-2966.2004.07611.x. arXiv:astro-ph/0309064
75. Mirabel, I.F., Rodriguez, L.F.: A superluminal source in the galaxy. Nature **371**, 46 (1994). doi:10.1038/371046a0
76. Mitrofanov, I.G.: Astrophysics (communication arising): a constraint on canonical quantum gravity? Nature **426**, 139 (2003)
77. Muleri, F.: On the operation of X-ray polarimeters with a large field of view. Submitted (2013)
78. Muleri, F., et al.: Feasibility of X-ray photoelectric polarimeters with large field of view. In: Bellazzini, R., Costa, E., Matt, G., Tagliaferri, G. (eds.) X-ray Polarimetry: A New Window in Astrophysics by Ronaldo Bellazzini, Enrico Costa, Giorgio Matt and Gianpiero Tagliaferri. Cambridge University Press. ISBN: 9780521191845, p. 72 (2010)
79. Muleri, F., Soffitta, P., Bellazzini, R., Brez, A., Costa, E., Fabiani, S., Frutti, M., Minuti, M., Negri, M.B., Pascale, P., Rubini, A., Sindoni, G., Spandre, G.: A very compact polarizer for an X-ray polarimeter calibration. In: Proceedings. SPIE, vol. 6686, p. 668610 (2007). doi:10.1117/12.734647
80. Muleri, F., Soffitta, P., Baldini, L., Bellazzini, R., Bregeon, J., Brez, A., Costa, E., Frutti, M., Latronico, L., Minuti, M., Negri, M.B., Omodei, N., Pesce-Rollins, M., Pinchera, M., Razzano, M., Rubini, A., Sgró, C., Spandre, G.: Low energy polarization sensitivity of the Gas Pixel

Detector. Nucl. Inst. Methods Phys. Res. A **584**, 149 (2008). doi:10.1016/j.nima.2007.09.046. arXiv:0709.4623
81. Muleri, F., Soffitta, P., Baldini, L., Bellazzini, R., Brez, A., Costa, E., Fabiani, S., Krummenacher, F., Latronico, L., Lazzarotto, F., Minuti, M., Pinchera, M., Rubini, A., Sgró, C., Spandre, G.: Spectral and polarimetric characterization of the Gas Pixel Detector filled with dimethyl ether. Nucl. Inst. Methods Phys. Res. A **620**, 285–293 (2010). arXiv:1003.6009
82. Muleri, F., Bellazzini, R., Brez, A., Costa, E., Fabiani, S., Minuti, M., Pinchera, M., Rubini, A., Soffitta, P., Spandre, G.: A new design for the gas pixel detector. In: Society of Photo-Optical Instrumentation Engineers (SPIE) Conference Series, Society of Photo-Optical Instrumentation Engineers (SPIE) Conference Series, vol. 8443 (2012). doi:10.1117/12.926006
83. Muno, M.P., Baganoff, F.K., Brandt, W.N., Park, S., Morris, M.R.: Discovery of variable iron fluorescence from reflection nebulae in the galactic center. ApJ **656**, L69–L72 (2007). doi:10.1086/512236. arXiv:astro-ph/0611651
84. Murakami, H., Koyama, K., Maeda, Y.: Chandra observations of diffuse X-rays from the sagittarius B2 cloud. ApJ **558**, 687–692 (2001). doi:10.1086/322282. arXiv:astro-ph/0105273
85. Murakami, H., Koyama, K., Tsujimoto, M., Maeda, Y., Sakano, M.: ASCA discovery of diffuse 6.4 KEV emission near the Sagittarius C complex: a new X-Ray reflection nebula. ApJ **550**, 297–300 (2001). doi:10.1086/319737. arXiv:astro-ph/0012310
86. Novick, R.: Stellar and solar X-ray polarimetry. Space Sci. Rev. **18**, 389 (1975). doi:10.1007/BF00212912
87. Novick, R., Weisskopf, M.C., Berthelsdorf, R., Linke, R., Wolff, R.S.: Detection of X-ray polarization of the crab nebula. ApJ **174**, L1 (1972)
88. Pacciani, L., Costa, E., Di Persio, G., Feroci, M., Soffitta, P., Baldini, L., Bellazzini, R., Brez, A., Lumb, N., Spandre, G.: Sensitivity of a photoelectric x-ray polarimeter for astronomy: the impact of the gas mixture and pressure. In: Proceedings SPIE, vol. 4843, p. 394 (2003)
89. Pavlov, G.G., Shibanov, I.A.: Thermal emission of an optically thick plasma containing a strong magnetic field. Soviet Ast. **22**, 214–222 (1978)
90. Pavlov, G.G., Zavlin, V.E.: Polarization of thermal X-rays from isolated neutron stars. ApJ **529**, 1011–1018 (2000). doi:10.1086/308313
91. Payez, A., Cudell, J.R., Hutsemékers, D.: New polarimetric constraints on axion-like particles. JCAP **7**, 041 (2012). doi:10.1088/1475-7516/2012/07/041. arXiv:1204.6187
92. Pearce, M., Florén, H.G., Jackson, M., Kamae, T., Kiss, M., Kole, M., Moretti, E., Olofsson, G., Rydström, S., Strömberg, J.E., Takahashi, H.: Balloon-borne hard X-ray polarimetry with PoGOLite (2012). arXiv:1211.5094
93. Peres, G., Reale, F., Serio, S., Pallavicini, R.: Hydrodynamic flare modeling - Comparison of numerical calculations with SMM observations of the 1980 November 12 17:00 UT flare. ApJ **312**, 895–908 (1987). doi:10.1086/164936
94. Perna, R., Ho, W.C.G., Verde, L., van Adelsberg, M., Jimenez, R.: Signatures of photon-axion conversion in the thermal spectra and polarization of neutron stars. ApJ **748**, 116 (2012). doi:10.1088/0004-637X/748/2/116. arXiv:1201.5390
95. Pierre Auger Collaboration, Abraham, J., Abreu, P., Aglietta, M., Aguirre, C., Allard, D., Allekotte, I., Allen, J., Allison, P., Alvarez, C., et al.: Correlation of the highest-energy cosmic rays with nearby extragalactic objects. Science **318**, 938 (2007). doi:10.1126/science.1151124. arXiv:0711.2256
96. Pierre Auger Collaboration, Abreu, P., Aglietta, M., Ahlers, M., Ahn, E.J., Albuquerque, I.F.M., Allard, D., Allekotte, I., Allen, J., Allison, P., et al: A search for anisotropy in the arrival directions of ultra high energy cosmic rays recorded at the Pierre Auger Observatory. JCAP **4**, 040 (2012). doi:10.1088/1475-7516/2012/04/040. arXiv:1210.3602
97. Poutanen, J.: Relativistic jets in blazars: polarization of radiation. ApJS **92**, 607–609 (1994). doi:10.1086/192024
98. Poutanen, J., Svensson, R.: The two-phase pair corona model for active galactic nuclei and X-Ray binaries: how to obtain exact solutions. ApJ **470**, 249 (1996). doi:10.1086/177865. arXiv:astro-ph/9605073
99. Poutanen, J., Vilhu, O.: Compton scattering of polarized light in two-phase accretion discs. A&A **275**, 337–344 (1993)
100. Poutanen, J., Nagendra, K.N., Svensson, R.: Green's matrix for Compton reflection of polarized radiation from cold matter. MNRAS **283**, 892–904 (1996)

101. Priest, E.R., Forbes, T.G.: The magnetic nature of solar flares. A&A Rev. **10**, 313–377 (2002). doi:10.1007/s001590100013
102. Reis, R.C., Miller, J.M., Reynolds, M.T., Fabian, A.C., Walton, D.J., Cackett, E., Steiner, J.F.: Evidence of light-bending effects and its implication for spectral state transitions. ApJ **763**, 48 (2013). doi:10.1088/0004-637X/763/1/48. arXiv:1208.3277
103. Reynoso, E.M., Hughes, J.P., Moffett, D.A.: On the radio polarization signature of efficient and inefficient particle acceleration in supernova remnant SN 1006. Astron. J. **145**(4), Article i.d. 104, 1–9 (2013). doi:10.1088/0004-6256/145/4/104. arXiv:1302.4678
104. Rossi, S., Homan, J., Miller, J.M., Belloni, T.: Iron-line and continuum flux variations in the RXTE spectra of the black hole candidate XTE J1650-500. MNRAS **360**, 763–768 (2005). doi:10.1111/j.1365-2966.2005.09069.x. arXiv:astro-ph/0504182
105. Saint-Hilaire, P., Krucker, S., Lin, R.P.: A statistical survey of hard X-ray spectral characteristics of solar flares with two footpoints. Sol. Phys. **250**, 53–73 (2008). doi:10.1007/s11207-008-9193-9. arXiv:1111.4247
106. Sanchez Almeida, J., Martinez Pillet, V.: Polarizing properties of grazing-incidence X-ray mirrors - Comment. Appl. Opt. **32**, 4231–4235 (1993). doi:10.1364/AO.32.004231
107. Sazonov, S.Y., Sunyaev, R.A.: Scattering in the inner accretion disk and the waveforms and polarization of millisecond flux oscillations in LMXBs. A&A **373**, 241–250 (2001). doi:10.1051/0004-6361:20010624. arXiv:astro-ph/0011352
108. Schnittman, J.D., Krolik, J.H.: X-ray polarization from accreting black holes: coronal emission. ApJ **712**, 908–924 (2010). doi:10.1088/0004-637X/712/2/908. arXiv:0912.0907
109. Seward, F.D.: Einstein observations of galactic supernova remnants. ApJS **73**, 781–819 (1990). doi:10.1086/191489
110. Shibata, S., Tomatsuri, H., Shimanuki, M., Saito, K., Mori, K.: On the X-ray image of the Crab nebula: comparison with Chandra observations. MNRAS **346**, 841 (2003). doi:10.1111/j.1365-2966.2003.07131.x. arXiv:astro-ph/0308422
111. Sidoli, L., Mereghetti, S., Treves, A., Parmar, A.N., Turolla, R., Favata, F.: X-ray emission from the giant molecular clouds in the Galactic Center region and the discovery of new X-ray sources. A&A **372**, 651–662 (2001). doi:10.1051/0004-6361:20010503. arXiv:astro-ph/0104121
112. Soffitta, P., Costa, E., Kaaret, P., Dwyer, J., Ford, E., Tomsick, J., Novick, R., Nenonen, S.: Proportional counters for the stellar X-ray polarimeter with a wedge and strip cathode pattern readout system. Nucl. Inst. Methods Phys. Res. A **414**, 218–232 (1998). doi:10.1016/S0168-9002(98)00572-5
113. Soffitta, P., Campana, R., Costa, E., Fabiani, S., Muleri, F., Rubini, A., Bellazzini, R., Brez, A., Minuti, M., Pinchera, M., Spandre, G.: The background of the gas pixel detector and its impact on imaging X-ray polarimetry. In: Society of Photo-Optical Instrumentation Engineers (SPIE) Conference Series, Society of Photo-Optical Instrumentation Engineers (SPIE) Conference Series, vol. 8443 (2012). doi:10.1117/12.925385
114. Soffitta, P., Muleri, F., Fabiani, S., Costa, E., Bellazzini, R., Brez, A., Minuti, M., Pinchera, M., Spandre, G.: Measurement of the position resolution of the Gas Pixel Detector. Nucl. Inst. Methods Phys. Res. A **700**, 99–105 (2013). doi:10.1016/j.nima.2012.09.055. arXiv:1208.6330
115. Spiga, D., et al.: Re-testing the Jet-X Flight Module No. 2 at the PANTER facility. In preparation (2013)
116. Stark, R.F., Connors, P.A.: Observational test for the existence of a rotating black hole in CYG X-1. Nature **266**, 429 (1977)
117. Stecker, F.W.: A new limit on Planck scale Lorentz violation from γ-ray burst polarization. Astropart. Phys. **35**, 95–97 (2011). doi:10.1016/j.astropartphys.2011.06.007. arXiv:1102.2784
118. Strohmayer, T.E., Kallman, T.R.: On the statistical analysis of X-ray polarization measurements. ApJ **773**, 103–112 (2013). doi:10.1088/0004-637X/773/2/103
119. Suarez-Garcia, E., Hajdas, W., Wigger, C., Arzner, K., Güdel, M., Zehnder, A., Grigis, P.: X-ray polarization of solar flares measured with Rhessi. Sol. Phys. **239**, 149–172 (2006). doi:10.1007/s11207-006-0268-1. arXiv:astro-ph/0609778
120. Sunyaev, R.A., Markevitch, M., Pavlinsky, M.: The center of the Galaxy in the recent past - A view from GRANAT. ApJ **407**, 606–610 (1993). doi:10.1086/172542
121. Swank, J., et al.: Gravity and Extreme Magnetism SMEX (GEMS). In: Bellazzini, R., Costa, E., Matt, G., Tagliaferri, G. (eds.) X-ray Polarimetry: A New Window in Astrophysics by Ronaldo Bellazzini, Enrico Costa, Giorgio Matt and Gianpiero Tagliaferri. Cambridge University Press. ISBN: 9780521191845, p. 251 (2010)

122. Sylwester, J., Kuzin, S., Kotov, Y.D., Farnik, F., Reale, F.: SphinX: A fast solar Photometer in X-rays. J. Astrophys. Astron. **29**, 339–343 (2008). doi:10.1007/s12036-008-0044-8
123. Tagliaferri, G., Hornstrup, A., Huovelin, J., Reglero, V., Romaine, S., Rozanska, A., Santangelo, A., Stewart, G.: The NHXM observatory. Exp. Astron. **34**, 463–488 (2012). doi:10.1007/s10686-011-9235-4
124. Tindo, I.P., Ivanov, V.D., Mandel'Stam, S.L., Shuryghin, A.I.: On the polarization of the emission of X-Ray solar flares. Sol. Phys. **14**, 204–207 (1970). doi:10.1007/BF00240179
125. Tindo, I.P., Ivanov, V.D., Mandel'Stam, S.L., Shuryghin, A.I.: New measurements of the polarization of X-Ray solar flares. Sol. Phys. **24**, 429–433 (1972). doi:10.1007/BF00153385
126. Tindo, I.P., Ivanov, V.D., Valníček, B., Livshits, M.A.: Preliminary interpretation of the polarization measurements performed on 'Intercosmos-4' during three X-Ray solar flares. Sol. Phys. **27**, 426–435 (1972). doi:10.1007/BF00153113
127. Toma, K., Mukohyama, S., Yonetoku, D., Murakami, T., Gunji, S., Mihara, T., Morihara, Y., Sakashita, T., Takahashi, T., Wakashima, Y., Yonemochi, H., Toukairin, N.: Strict limit on CPT violation from polarization of γ-Ray bursts. Phys. Rev. Lett. **109**(24), 241104 (2012). doi:10.1103/PhysRevLett.109.241104. arXiv:1208.5288
128. Tomsick, J., Costa, E., Dwyer, J., Elsner, R.F., Ford, E., Kaaret, P.E., Novick, R., Santangelo, A.E., Silver, E., Soffitta, P., Weisskopf, M.C., Ziock, K.P.: Calibration of the stellar X-ray polarimeter. In: Siegmund, O.H., Gummin, M.A. (eds.) Society of Photo-Optical Instrumentation Engineers (SPIE) Conference Series, Society of Photo-Optical Instrumentation Engineers (SPIE) Conference Series, vol. 3114, pp. 373–383 (1997)
129. Tramiel, L.J., Novick, R., Chanan, G.A.: Polarization evidence for the isotropy of electrons responsible for the production of 5-20 keV X-rays in solar flares. ApJ **280**, 440–447 (1984). doi:10.1086/162010
130. van Adelsberg, M., Lai, D.: Atmosphere models of magnetized neutron stars: QED effects, radiation spectra and polarization signals. MNRAS **373**, 1495–1522 (2006). doi:10.1111/j.1365-2966.2006.11098.x. arXiv:astro-ph/0607168
131. van Adelsberg, M., Perna, R.: Soft X-ray polarization in thermal magnetar emission. MNRAS **399**, 1523–1533 (2009). doi:10.1111/j.1365-2966.2009.15374.x. arXiv:0907.3499
132. Viironen, K., Poutanen, J.: Light curves and polarization of accretion- and nuclear-powered millisecond pulsars. A&A **426**, 985–997 (2004). doi:10.1051/0004-6361:20041084. arXiv:astro-ph/0408250
133. Vink, J.: Supernova remnants: the X-ray perspective. A&A Rev. **20**, 49 (2012). doi:10.1007/s00159-011-0049-1. arXiv:1112.0576
134. Volpi, D., Del Zanna, L., Amato, E., Bucciantini, N.: Polarization in Pulsar Wind Nebulae (2009). arXiv: 0903.4120
135. Weisskopf, M.C., Cohen, G.G., Kestenbaum, H.L., Long, K.S., Novick, R., Wolff, R.S.: Measurement of the X-ray polarization of the Crab Nebula. ApJ **208**, L125 (1976)
136. Weisskopf, M.C., Silver, E.H., Kestenbaum, H.L., Long, K.S., Novick, R., Wolff, R.S.: Search for X-ray polarization in Cygnus X-1. ApJ **215**, L65–L68 (1977). doi:10.1086/182479
137. Weisskopf, M.C., Kestenbaum, H.L., Long, K.S., Novick, R., Silver, E.H.: An upper limit to the linear X-ray polarization of Scorpius X-1. ApJ **221**, L13–L16 (1978). doi:10.1086/182655
138. Weisskopf, M.C., Silver, E.H., Kestenbaum, H.L., Long, K.S., Novick, R.: A precision measurement of the X-ray polarization of the Crab Nebula without pulsar contamination. ApJ **220**, L117 (1978). doi:10.1086/182648
139. Weisskopf, M.C., Elsner, R.F., O'Dell, S.L.: On understanding the figures of merit for detection and measurement of x-ray polarization. In: Society of Photo-Optical Instrumentation Engineers (SPIE) Conference Series, Society of Photo-Optical Instrumentation Engineers (SPIE) Conference Series, vol. 7732 (2010). doi:10.1117/12.857357
140. Weisskopf, V.C.: ber die Elektrodynamik des Vakuums auf Grund der Quantentheorie des Elektrons. Det Kgl Danske Viden Selskab Mat fys Medd XIV **6**, 1–36 (1936)
141. Wells, A.A., Castelli, C.M., Denby, M., Pullan, D., Sims, M.R., Watson, D.J., Whitford, C.H., Willingale, R., Eyles, C.J., Cooke, M., Curtis, W.J., Braeuninger, H.W., Burket, W., Egger, R., Citterio, O., Campana, S., Cusumano, G.: X-ray imaging performance of the flight model JET-X telescope. In: Siegmund, O.H., Gummin, M.A. (eds.) Society of Photo-Optical Instrumentation Engineers (SPIE) Conference Series, Society of Photo-Optical Instrumentation Engineers (SPIE) Conference Series, vol. 3114, pp. 392–403 (1997)

142. Yonetoku, D., Murakami, T., Gunji, S., Mihara, T., Sakashita, T., Morihara, Y., Kikuchi, Y., Takahashi, T., Fujimoto, H., Toukairin, N., Kodama, Y., Kubo, S., Ikaros Demonstration Team: Gamma-ray burst polarimeter (GAP) aboard the small solar power sail demonstrator IKAROS. PASJ **63**, 625 (2011). arXiv:1010.5305
143. Yonetoku, D., Murakami, T., Gunji, S., Mihara, T., Toma, K., Morihara, Y., Takahashi, T., Wakashima, Y., Yonemochi, H., Sakashita, T., Toukairin, N., Fujimoto, H., Kodama, Y.: Magnetic structures in gamma-ray burst jets probed by gamma-ray polarization. ApJ **758**, L1 (2012). doi:10.1088/2041-8205/758/1/L1. arXiv:1208.5287
144. Zavattini, E., Zavattini, G., Ruoso, G., Polacco, E., Milotti, E., Karuza, M., Gastaldi, U., di Domenico, G., Della Valle, F., Cimino, R., Carusotto, S., Cantatore, G., Bregant, M.: Experimental observation of optical rotation generated in vacuum by a magnetic field. Phys. Rev. Lett. **96**(11), 110406 (2006). doi:10.1103/PhysRevLett.96.110406. arXiv:hep-ex/0507107
145. Zavattini, E., Zavattini, G., Ruoso, G., Raiteri, G., Polacco, E., Milotti, E., Lozza, V., Karuza, M., Gastaldi, U., di Domenico, G., Della Valle, F., Cimino, R., Carusotto, S., Cantatore, G., Bregant, M.: New PVLAS results and limits on magnetically induced optical rotation and ellipticity in vacuum. Phys. Rev. D **77**(3), 032006 (2008). doi:10.1103/PhysRevD.77.032006. arXiv:0706.3419
146. Zavattini, G., Gastaldi, U., Pengo, R., Ruoso, G., Valle, F.D., Milotti, E.: Measuring the magnetic birefringence of vacuum: the Pvlas experiment. Int. J. Modern Phys. A **27**, 1260017 (2012). doi:10.1142/S0217751X12600172. arXiv:1201.2309
147. Zharkova, V.V., Kuznetsov, A.A., Siversky, T.V.: Diagnostics of energetic electrons with anisotropic distributions in solar flares. I. Hard X-rays bremsstrahlung emission. A&A **512**, A8 (2010). doi:10.1051/0004-6361/200811486
148. Zhitnik, I.A., Logachev, Y.I., Bogomolov, A.V., Denisov, Y.I., Kavanosyan, S.S., Kuznetsov, S.N., Morozov, O.V., Myagkova, I.N., Svertilov, S.I., Ignat'ev, A.P., Oparin, S.N., Pertsov, A.A., Tindo, I.P.: Polarization, temporal, and spectral parameters of solar flare hard X-rays as measured by the SPR-N instrument onboard the CORONAS-F satellite. Solar Syst. Res. **40**, 93–103 (2006). doi:10.1134/S003809460602002X